

Energy conserving SUPG methods for compatible finite element schemes in numerical weather prediction

Golo A. Wimmer^{1*}, Colin J. Cotter¹ and Werner Bauer^{1,2}

¹*Imperial College London*, ²*INRIA Rennes*

*Correspondence to: gaw16@ic.ac.uk

Friday 12th November, 2021

Abstract

We present an energy conserving space discretisation based on a Poisson bracket that can be used to derive the dry compressible Euler as well as thermal shallow water equations. It is formulated using the compatible finite element method, and extends the incorporation of upwinding for the shallow water equations as described in Wimmer, Cotter, and Bauer (2019). While the former is restricted to DG upwinding, an energy conserving SUPG scheme for the (partially) continuous Galerkin thermal field space is newly introduced here. The energy conserving property is validated by coupling the Poisson bracket based spatial discretisation to an energy conserving time discretisation. Further, the discretisation is demonstrated to lead to an improved temperature field development with respect to stability when upwinding is included. An approximately energy conserving full discretisation with a smaller computational cost is also presented.

Keywords: Compatible finite element methods; Hamiltonian mechanics; Poisson bracket; SUPG method

1 Introduction

Finite element methods have recently gained an increased interest in numerical weather prediction (NWP), as they allow for higher order discretisations and more general meshes, thus avoiding the parallel computing issues associated with grid poles. This includes spectral element methods, discontinuous Galerkin methods, and the compatible finite element method [7], where in the latter finite element spaces are mapped to one another via differential operators [20]. In the context of NWP, the compatible finite element method can be seen as an extension of the Arakawa C finite difference grid, and a dynamical core based on it is currently in development at the UK Met Office [9], due to replace the current finite difference latitude longitude mesh discretisation.

An important aspect of discretisations in NWP, particularly for climate simulations, is conservation of quantities such as mass and energy. While the former can be conserved using a suitable discretisation of the continuity equation, the latter requires a careful discretisation of all prognostic equations, ensuring that the energy losses and gains are balanced between the discretised terms. One way to guide this process is to consider the equations in a Hamiltonian framework [18], where the Hamiltonian is given by the system's total energy, and the equations are inferred by a Poisson bracket. Conservation of energy then follows directly from the bracket's antisymmetry, and any space discretisation maintaining this property will then also conserve energy. In particular, this framework facilitates the construction of advection schemes, which may otherwise not have an easily accountable effect on the total energy development. For the dry compressible Euler equations,

which form the basic equation set of dynamical cores in NWP, such Hamiltonian based discretisations already exist e.g. for hexagonal finite difference C-grids [10] (which includes higher order transport schemes) and the compatible finite element method [14].

For finite element methods, the choice of advection scheme depends on the underlying space, and for the compatible finite element method, this requires different formulations for the range of different spaces in use, including continuous and discontinuous ones. Within the Poisson bracket framework, DG upwinding for the depth field in the rotating shallow water equations as well as for the buoyancy field in the thermal shallow water equations has already been introduced in [26] and [8], respectively. Further, an upwinded energy conserving velocity advection scheme was presented in the context of Lie derivatives for the incompressible Euler equations in [19], which was extended to the shallow water case in [20] and the shallow water case from a Poisson bracket point of view in [26]. Finally, an energy conserving SUPG advection scheme was considered for potential vorticity advection in the shallow water equations in [1], exploiting the fact that the Poisson bracket term corresponding to velocity advection is antisymmetric in itself.

These energy conserving upwinded advection schemes can, with the exception of the potential vorticity scheme, in principle be implemented readily for the three-dimensional dry compressible Euler equations. However, an upwinded, energy conserving potential temperature advection scheme is still missing if a continuous (or partially continuous) finite element space is used for the temperature field. In particular, this is the case for the finite element equivalent of a Charney-Phillips finite difference grid, where the space's node locations are set to coincide with the velocity space nodes corresponding to the vertical velocity [20]. This choice of temperature space was recommended in a dispersion property study in [16] for mixed finite element methods in NWP when compared to a fully discontinuous or fully continuous finite element space, and will be used in the UK Met Office's next dynamical core.

Advection terms for fields in continuous or partially continuous finite element spaces can be discretised using the Streamline Upwind Petrov Galerkin (SUPG) method [4], where a diffusive term is added along the direction of the flow to all test functions. In this paper, we present a discretised almost-Poisson bracket that includes SUPG upwinding for the thermal field, which, depending on the choice of Hamiltonian, leads to an energy conserving space discretisation for the dry compressible Euler equations or the thermal shallow water equations. The energy conservation property as well as the thermal field's qualitative development are then verified in numerical test cases, using an energy conserving time discretisation as described in [6]. For simplicity, while the formulation is valid in three dimensions, we consider two-dimensional scenarios in this paper. This includes vertical slice test cases of the Euler equations with a Charney-Phillips type temperature space, as well as a spherical test case of the thermal shallow water equations with a fully continuous buoyancy space. Further, in view of the increased computational cost to achieve energy conservation to machine precision, we also consider a simplified discretisation, which relies on an approximation to the Poisson integrator and a small adjustment in the almost Poisson bracket. To arrive at a fully upwinded bracket, the latter additionally includes upwinding in density and velocity.

The rest of the paper is structured as follows: In Section 2, we review the Poisson bracket as well as the SUPG scheme, and present the space discretised formulation including upwinding. In Section 3, we describe the full discretisation, introduce the simplified discretised form, and present numerical results. Finally, in Section 4, we review the formulation and the corresponding numerical results, and discuss ongoing work.

2 Formulation

In this section, we first review the Poisson bracket, which we present in its continuous form. We then describe how to derive the resulting sets of equations, considering Hamiltonians that lead to the dry compressible Euler and the thermal shallow water equations. Next, we describe the finite element space discretisation, including the Streamline Upwind Petrov Galerkin stabilisation scheme for advection terms, as well as a mixed SUPG/DG upwinding scheme for the Charney-Phillips type finite element space, as described in [20]. Finally, we derive a set of upwinded equations within the Poisson bracket framework, and further discuss how to incorporate existing upwinding schemes for the velocity and density fields in the bracket.

2.1 Hamiltonian formulation

Many fluid dynamical equations can be formulated within a Hamiltonian framework, using the system's Hamiltonian H , i.e. the total amount of energy, and a Poisson bracket $\{.,.\}$, which is an antisymmetric bilinear form that satisfies the Jacobi identity (for more details, see [22]). The time evolution of any functional F of the prognostic variables is then given by

$$\frac{dF}{dt} = \{F, H\}. \quad (2.1.1)$$

Here, we consider prognostic variables \mathbf{u} , ρ , and θ in a two-dimensional domain Ω , which denote the flow velocity, a density related field, and a thermal type field, respectively. Further, we use a bracket of form

$$\{F, H\} := -\left\langle \frac{\delta F}{\delta \mathbf{u}}, \mathbf{q} \times \frac{\delta H}{\delta \mathbf{u}} \right\rangle + \left\langle \frac{\delta H}{\delta \rho}, \nabla \cdot \frac{\delta F}{\delta \mathbf{u}} \right\rangle + \left\langle \frac{1}{\rho} \frac{\delta H}{\delta \theta} \nabla \theta, \frac{\delta F}{\delta \mathbf{u}} \right\rangle \quad (2.1.2)$$

$$- \left\langle \frac{\delta F}{\delta \rho}, \nabla \cdot \frac{\delta H}{\delta \mathbf{u}} \right\rangle - \left\langle \frac{1}{\rho} \frac{\delta F}{\delta \theta} \nabla \theta, \frac{\delta H}{\delta \mathbf{u}} \right\rangle, \quad (2.1.3)$$

for L2 inner product $\langle ., . \rangle$. \mathbf{q} denotes a vorticity type variable, given by

$$\mathbf{q} = (\nabla \times \mathbf{u} + 2\mathbf{\Omega})/\rho, \quad (2.1.4)$$

for rotation vector $\mathbf{\Omega}$. Note that in the two-dimensional test cases considered in the numerical results section below, \mathbf{q} corresponds to a scalar vorticity field q multiplied by the 2D domain's outward unit vector, with q given by

$$q = (\nabla^\perp \cdot \mathbf{u} + f)/\rho, \quad (2.1.5)$$

for 2D curl $\nabla^\perp = (-\partial_y, \partial_x)$ and Coriolis parameter f depending on the test case. The functional derivatives appearing in the bracket are defined weakly by

$$\left\langle \frac{\delta F}{\delta \mathbf{u}}, \mathbf{w} \right\rangle := \lim_{\epsilon \rightarrow 0} \frac{1}{\epsilon} (F(\mathbf{u} + \epsilon \mathbf{w}, D) - F(\mathbf{u}, D)) \quad \forall \mathbf{w} \in V(\Omega), \quad (2.1.6)$$

for a suitable space $V(\Omega)$ to be defined, and similar for ρ and θ . In the continuous setting, we consider continuously differentiable spaces for V , which are then discretised using suitable finite element spaces. The resulting fluid dynamical equations follow from their respective Hamiltonians and functionals F corresponding to weak forms of the prognostic variables, i.e. $F = \langle \mathbf{u}, \mathbf{v} \rangle$, $F = \langle \rho, \psi \rangle$, and $F = \langle \theta, \chi \rangle$, respectively, for arbitrary test functions \mathbf{v}, ψ, χ in the corresponding spaces $V(\Omega)$. For $F = \langle \mathbf{u}, \mathbf{v} \rangle$, we have

$$\frac{\delta F}{\delta \mathbf{u}} = \mathbf{v}, \quad \frac{\delta F}{\delta \rho} = 0, \quad \frac{\delta F}{\delta \theta} = 0, \quad (2.1.7)$$

so that the Poisson bracket reduces to

$$\{F, H\} = -\langle \mathbf{v}, \mathbf{q} \times \frac{\delta H}{\delta \mathbf{u}} \rangle + \langle \frac{\delta H}{\delta \rho}, \nabla \cdot \mathbf{v} \rangle + \langle \frac{1}{\rho} \frac{\delta H}{\delta \theta} \nabla \theta, \mathbf{v} \rangle, \quad (2.1.8)$$

for any test function $\mathbf{v} \in V(\Omega)$. Using the Poisson system (2.1.1), we then obtain a momentum equation given by

$$\langle \mathbf{v}, \mathbf{u}_t \rangle = \frac{dF}{dt} = -\langle \mathbf{v}, \mathbf{q} \times \frac{\delta H}{\delta \mathbf{u}} \rangle + \langle \frac{\delta H}{\delta \rho}, \nabla \cdot \mathbf{v} \rangle + \langle \frac{1}{\rho} \frac{\delta H}{\delta \theta} \nabla \theta, \mathbf{v} \rangle, \quad (2.1.9)$$

where the subscript in t denotes differentiation with respect to t . Similarly, for ρ and θ , we obtain weak versions of the continuity and transport equations of form

$$\langle \psi, \rho_t \rangle = -\langle \psi, \nabla \cdot \frac{\delta H}{\delta \mathbf{u}} \rangle, \quad (2.1.10)$$

$$\langle \chi, \theta_t \rangle = -\langle \chi, \frac{1}{\rho} \frac{\delta H}{\delta \mathbf{u}} \cdot \nabla \theta \rangle, \quad (2.1.11)$$

for any test functions ψ, χ . Given a system of equations of form (2.1.9) - (2.1.11), conservation of energy then follows directly from the bracket framework. First, the Poisson system (2.1.1) with bracket (2.1.2) - (2.1.3) can be recovered from (2.1.9) - (2.1.11) for any functional $F(\mathbf{u}, \rho, \theta)$ via

$$\frac{dF}{dt} = \langle \frac{\delta F}{\delta \mathbf{u}}, \mathbf{u}_t \rangle + \langle \frac{\delta F}{\delta \rho}, \rho_t \rangle + \langle \frac{\delta F}{\delta \theta}, \theta_t \rangle = \{F, H\}. \quad (2.1.12)$$

In particular, this also holds for $F = H$, and noting the bracket's antisymmetry, we arrive at

$$\frac{dH}{dt} = \{H, H\} = -\{H, H\} = 0. \quad (2.1.13)$$

2.1.1 Euler equations

A Poisson bracket based formulation of the dry compressible Euler equations can be found e.g. in [10, 14]. Note that the Poisson bracket and the skew symmetric operator presented in these papers correspond to a different Poisson bracket to the one considered here, relying on the use of a different set of underlying fields (with mass weighted potential temperature Θ). In our case, the Hamiltonian is given by

$$H(\mathbf{u}, \rho, \theta) = \int_{\Omega} \left(\frac{\rho}{2} |\mathbf{u}|^2 + g\rho z + c_v \rho \theta \pi \right) dx, \quad (2.1.14)$$

for wind velocity \mathbf{u} , air density ρ , and potential temperature θ . z , g and c_v denote the vertical coordinate, gravitational acceleration and specific heat of air at constant volume, respectively. Further, π denotes the Exner pressure, which is given by the ideal gas law as

$$\pi^{\frac{1-\kappa}{\kappa}} = \frac{R}{p_0} \rho \theta, \quad (2.1.15)$$

for reference pressure p_0 , ideal gas constant R , and non-dimensional parameter $\kappa = R/c_p$, where $c_p = R + c_v$ denotes the specific heat at constant pressure. In view of the Poisson system (2.1.1), in the non-discretised case the variational derivatives are given by

$$\frac{\delta H}{\delta \mathbf{u}} = \rho \mathbf{u}, \quad \frac{\delta H}{\delta \rho} = \frac{1}{2} |\mathbf{u}|^2 + gz + c_p \theta \pi, \quad (2.1.16)$$

$$\frac{\delta H}{\delta \theta} = c_p \rho \pi, \quad (2.1.17)$$

where we used (2.1.15) to derive the pressure related expressions for the variations in ρ and θ . The usual form of the Euler equations then follows from (2.1.9) - (2.1.11). For the velocity equation, we have

$$\langle \mathbf{v}, \mathbf{u}_t \rangle = -\langle \mathbf{v}, \mathbf{q} \times \frac{\delta H}{\delta \mathbf{u}} \rangle + \langle \frac{\delta H}{\delta \rho}, \nabla \cdot \mathbf{v} \rangle + \langle \frac{1}{\rho} \frac{\delta H}{\delta \theta} \nabla \theta, \mathbf{v} \rangle \quad (2.1.18)$$

$$= -\langle \mathbf{v}, \mathbf{q} \times (\rho \mathbf{u}) \rangle + \langle \frac{1}{2} |\mathbf{u}|^2 + gz + c_p \theta \pi, \nabla \cdot \mathbf{v} \rangle + \langle c_p \pi \nabla \theta, \mathbf{v} \rangle \quad (2.1.19)$$

$$= -\langle \mathbf{v}, (\nabla \times \mathbf{u} + 2\mathbf{\Omega}) \times \mathbf{u} \rangle - \langle \frac{1}{2} \nabla |\mathbf{u}|^2 + g\mathbf{k} + c_p \nabla(\theta \pi) \rangle + \langle c_p \pi \nabla \theta, \mathbf{v} \rangle \quad (2.1.20)$$

$$= -\langle \mathbf{v}, (\mathbf{u} \cdot \nabla) \mathbf{u} + 2\mathbf{\Omega} \times \mathbf{u} + g\mathbf{k} + c_p \theta \nabla \pi \rangle, \quad (2.1.21)$$

for vertical unit vector \mathbf{k} , and where we have used integration by parts (with $\mathbf{v} \cdot \mathbf{n} = 0$ on $\partial\Omega$) and $(\mathbf{u} \cdot \nabla) \mathbf{u} = (\nabla \times \mathbf{u}) \times \mathbf{u} + \frac{1}{2} \nabla |\mathbf{u}|^2$. Since this holds for any test function \mathbf{v} in $C^1(\Omega)$, we arrive at the usual strong form of the momentum equation given by

$$\mathbf{u}_t + (\mathbf{u} \cdot \nabla) \mathbf{u} + 2\mathbf{\Omega} \times \mathbf{u} + g\mathbf{k} + c_p \theta \nabla \pi = 0. \quad (2.1.22)$$

Similarly, we obtain the continuity and temperature transport equations of form

$$\rho_t + \nabla \cdot (\rho \mathbf{u}) = 0, \quad (2.1.23)$$

$$\theta_t + \mathbf{u} \cdot \nabla \theta = 0, \quad (2.1.24)$$

where we used $\frac{\delta H}{\delta \mathbf{u}} = \rho \mathbf{u}$ in (2.1.10) and (2.1.11), which hold for any test functions ψ and χ , respectively.

2.1.2 Thermal shallow water equations

For the thermal shallow water equations, we follow [8] and consider a Hamiltonian of form

$$H(\mathbf{u}, \rho, \theta) = \int_{\Omega} \left(\frac{\rho}{2} |\mathbf{u}|^2 + \rho \theta \left(\frac{\rho}{2} + b \right) \right) dx, \quad (2.1.25)$$

where in this context ρ corresponds to the fluid height (and for consistency of notation, we keep ρ instead of using the more usual D or h), and θ to the buoyancy. Further, b denotes the topographic height. The Hamiltonian variations are now given by

$$\frac{\delta H}{\delta \mathbf{u}} = \rho \mathbf{u}, \quad \frac{\delta H}{\delta \rho} = \frac{1}{2} |\mathbf{u}|^2 + \theta(\rho + b), \quad (2.1.26)$$

$$\frac{\delta H}{\delta \theta} = \rho \left(\frac{\rho}{2} + b \right), \quad (2.1.27)$$

and we obtain a weak momentum equation of form

$$\langle \mathbf{v}, \mathbf{u}_t \rangle = -\langle \frac{\delta F}{\delta \mathbf{u}}, \mathbf{q} \times \frac{\delta H}{\delta \mathbf{u}} \rangle + \langle \frac{\delta H}{\delta \rho}, \nabla \cdot \frac{\delta F}{\delta \mathbf{u}} \rangle + \langle \frac{1}{\rho} \frac{\delta H}{\delta \theta} \nabla \theta, \frac{\delta F}{\delta \mathbf{u}} \rangle \quad (2.1.28)$$

$$= -\langle \mathbf{v}, \mathbf{q} \times (\rho \mathbf{u}) \rangle + \langle \frac{1}{2} |\mathbf{u}|^2 + \theta(\rho + b), \nabla \cdot \mathbf{v} \rangle + \langle \left(\frac{\rho}{2} + b \right) \nabla \theta, \mathbf{v} \rangle \quad (2.1.29)$$

$$= -\langle \mathbf{v}, (\nabla \times \mathbf{u}) \times \mathbf{u} \rangle - \langle \mathbf{v}, 2\mathbf{\Omega} \times \mathbf{u} \rangle \quad (2.1.30)$$

$$- \langle \frac{1}{2} \nabla |\mathbf{u}|^2 + \nabla(\theta(\rho + b)), \mathbf{v} \rangle + \langle \left(\frac{\rho}{2} + b \right) \nabla \theta, \mathbf{v} \rangle \quad (2.1.31)$$

$$= -\langle \mathbf{v}, (\mathbf{u} \cdot \nabla) \mathbf{u} + (2\mathbf{\Omega} \times \mathbf{u}) + \theta \nabla(\rho + b) + \frac{\rho}{2} \nabla \theta \rangle, \quad (2.1.32)$$

In the non-discretised case, this leads to

$$\mathbf{u}_t + (\mathbf{u} \cdot \nabla) \mathbf{u} + f \mathbf{u}^\perp + \theta \nabla(\rho + b) + \frac{\rho}{2} \nabla \theta = 0, \quad (2.1.33)$$

noting that given the spherical context of the shallow water equations, we rewrote the Coriolis term as $f \mathbf{u}^\perp$, for Coriolis parameter $f = 2\Omega z/a$ and perpendicular $\mathbf{u}^\perp = \mathbf{k} \times \mathbf{u}$, where a , Ω , z , and \mathbf{k} correspond to the sphere's radius, rotation rate, rotational axis coordinate, and unit vertical vector, respectively. Similarly, as in the Euler case, equations for ρ and θ follow from (2.1.10) and (2.1.11), and since the variational derivative $\frac{\delta H}{\delta \mathbf{u}}$ is the same here, the resulting equations are given as before by

$$\rho_t + \nabla \cdot (\rho \mathbf{u}) = 0, \quad (2.1.34)$$

$$\theta_t + \mathbf{u} \cdot \nabla \theta = 0. \quad (2.1.35)$$

2.2 Space discretisation

In this section, we describe the space discretisation for the Poisson bracket introduced above. First, we discuss our choice of compatible finite element spaces for the fields \mathbf{u} , ρ , and q , as well as the additional space for the thermal field θ . Next, we describe SUPG stabilised schemes for the advection of θ and present the incorporation of these schemes into the Poisson bracket framework, which forms the core part of this paper. Finally, we discuss how to include upwinding for \mathbf{u} and ρ in this bracket, as presented in [26].

2.2.1 Choice of compatible finite element spaces

To discretise (2.1.9) - (2.1.11) and the diagnostic vorticity equation (2.1.5), we consider compatible finite element spaces for \mathbf{u} , ρ , and q . They are given by \mathbb{V}_q , \mathbb{V}_u , and \mathbb{V}_ρ such that

$$\mathbb{V}_q \xrightarrow{\nabla^\perp} \mathbb{V}_u \xrightarrow{\nabla} \mathbb{V}_\rho, \quad (2.2.1)$$

that is the differential operators appearing in our equations map one finite element space to another. In the case of the Euler equations, where we consider a (horizontally periodic) vertical slice of the atmosphere, the spaces are based on tensor products of continuous Galerkin (CG) and discontinuous Galerkin (DG) finite elements defined on intervals and are given by [20]

$$\mathbb{V}_q = CG_{r+1}(T) \otimes CG_{s+1}(S) \quad (2.2.2)$$

$$\mathbb{V}_u = [DG_r(T) \mathbf{k} \otimes CG_{s+1}(S)] \oplus [CG_{r+1}(T) \otimes DG_s(S) \mathbf{k}], \quad (2.2.3)$$

$$\mathbb{V}_\rho = DG_r \otimes DG_s(S), \quad (2.2.4)$$

where T , S denote horizontal and vertical reference intervals, respectively. In the numerical results section below, we will set $r = s$ and use bilinear ($r = 1$) and biquadratic ($r = 2$) finite elements for the density space. The corresponding compatible finite elements for $r = 1$ are depicted in Figure 1. Note that in three dimensions, we would consider compatible horizontal reference cells instead of intervals in the tensor product. The discretisation described below is still valid in the 3D case, except that the diagnostic scalar vorticity equation would be replaced by its corresponding vector field form.

For the thermal shallow water equations, where we consider triangular spherical meshes, we follow [26] and use the degree two Brezzi-Douglas-Marini finite element space BDM_2 for the velocity field. The compatible depth and vorticity spaces are then given by P_1^{DG} and P_3 , i.e. the first and third

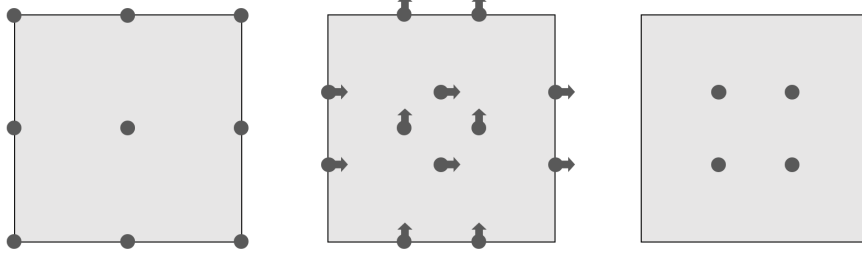


Figure 1: Vertical slice reference elements for next to lowest order compatible spaces for \mathbb{V}_q , $\mathbb{V}_{\mathbf{u}}$, and \mathbb{V}_ρ . Dots and arrows denote degrees of freedom and degrees of freedom multiplied by horizontal/vertical unit vectors, respectively.

(polynomial) order discontinuous and continuous triangular Galerkin spaces, respectively.

Finally, we need to specify finite element spaces for the thermal field θ . In the case of the thermal shallow water equations, we use the continuous space \mathbb{V}_q , given by P_3 . For the Euler equations, we consider a Charney-Phillips (CP) type space by choosing the finite element nodes to coincide with the vertical wind nodes of the velocity space element. The resulting elements for the thermal field space in the case of the Euler and thermal shallow water equations are given in Figure 2.

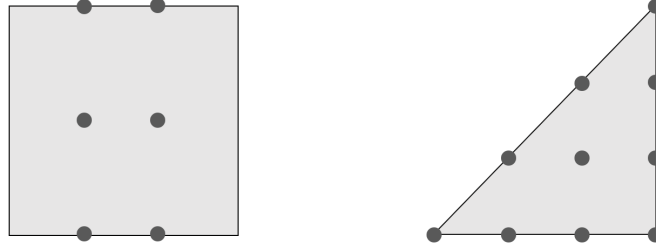


Figure 2: Reference elements for next to lowest order Charney-Phillips type finite element space and P_3 . Dots denote degrees of freedom. The former is used for the Euler equations in a vertical slice of the atmosphere; the latter corresponds to a triangular mesh of the sphere used for the thermal shallow water equations.

In terms of the equations derived by the Poisson bracket in Section 2.1, we obtain a space discretisation given by

$$\langle \mathbf{w}, \mathbf{u}_t \rangle + \langle \mathbf{w}, \mathbf{q} \times \frac{\delta H}{\delta \mathbf{u}} \rangle - \langle \frac{\delta H}{\delta \rho}, \nabla \cdot \mathbf{w} \rangle - \langle \frac{1}{\rho} \frac{\delta H}{\delta \theta} \nabla \theta, \mathbf{w} \rangle = 0 \quad \forall \mathbf{w} \in \mathbb{V}_u, \quad (2.2.5)$$

$$\langle \phi, \rho_t \rangle + \langle \phi, \nabla \cdot \frac{\delta H}{\delta \mathbf{u}} \rangle = 0 \quad \forall \phi \in \mathbb{V}_\rho, \quad (2.2.6)$$

$$\langle \gamma, \theta_t \rangle + \langle \gamma, \frac{1}{\rho} \frac{\delta H}{\delta \mathbf{u}} \cdot \nabla \theta \rangle = 0 \quad \forall \gamma \in \mathbb{V}_\theta, \quad (2.2.7)$$

together with a discretised diagnostic scalar vorticity equation given by

$$\langle \eta, q\rangle = -\langle \nabla^\perp \eta, \mathbf{u} \rangle + \langle \langle \eta, \mathbf{n}^\perp \cdot \mathbf{u} \rangle \rangle + \langle \eta, f \rangle \quad \forall \eta \in \mathbb{V}_q, \quad (2.2.8)$$

for L2 inner product $\langle \cdot, \cdot \rangle$ on $\partial\Omega$. Note that the variational derivatives of H are now given by projections into the relevant finite element spaces, e.g. for the Hamiltonian corresponding to the

Euler equations, we find

$$\frac{\delta H}{\delta \mathbf{u}} = P_{\mathbb{V}_{\mathbf{u}}}(\rho \mathbf{u}), \quad \frac{\delta H}{\delta \rho} = P_{\mathbb{V}_{\rho}}\left(\frac{1}{2}|\mathbf{u}|^2 + gz + c_p \theta \pi\right), \quad (2.2.9)$$

$$\frac{\delta H}{\delta \theta} = P_{\mathbb{V}_{\theta}}(\rho c_p \pi), \quad (2.2.10)$$

where $P_{\mathbb{V}}$ denotes projection into \mathbb{V} . Further, we note that the Poisson bracket structure still holds in the discretised case, i.e. the discretised evolution equations (2.2.5) - (2.2.7) can be used for evaluating dF/dt as in (2.1.12), leading to a Poisson system (as in (2.1.1)) with a bracket whose form is equal to the continuous one, given by (2.1.2) - (2.1.3). While it is not clear if the discretised bracket still satisfies the Jacobi identity, it is still antisymmetric, implying that energy is conserved. We therefore find that the discretised bracket is at least an almost Poisson bracket, i.e. a bilinear antisymmetric form.

2.3 SUPG stabilisation

To review the SUPG advection scheme, we consider the thermal field transport equation in its continuous form, given by

$$\theta_t + \mathbf{u} \cdot \nabla \theta = 0. \quad (2.3.1)$$

In a finite element setting, we would then space discretise using its weak form

$$\langle \gamma, \theta_t \rangle + \langle \gamma, \mathbf{u} \cdot \nabla \theta \rangle = 0 \quad \forall \gamma \in \mathbb{V}_{\theta}. \quad (2.3.2)$$

However, for standard continuous Galerkin spaces, the advection term tends to produce spurious oscillations, which can be counteracted by introducing diffusion in the direction of the flow [13]. This is achieved by replacing the test functions by

$$\gamma \rightarrow \gamma + \tau \mathbf{u} \cdot \nabla \gamma =: \gamma_{\mathbf{u}}, \quad (2.3.3)$$

for a suitable coefficient τ . We then arrive at

$$\langle \gamma_{\mathbf{u}}, \theta_t + \mathbf{u} \cdot \nabla \theta \rangle = 0 \quad \forall \gamma \in \mathbb{V}_{\theta}, \quad (2.3.4)$$

and this form of upwinding is commonly referred to as the Streamline Upwind Petrov Galerkin (SUPG) method [13], and was first introduced in [4]. We find that the modified test function of the advection term acts as diffusion along the velocity field \mathbf{u} , noting that for $\gamma = \theta \in \mathbb{V}_{\theta}$, the SUPG equation (2.3.4) leads to

$$\frac{1}{2} \frac{\partial}{\partial t} \|\theta\|_2^2 = -\langle \theta, \mathbf{u} \cdot \nabla \theta \rangle - \|\sqrt{\tau} \mathbf{u} \cdot \nabla \theta\|_2^2 - \tau \langle \mathbf{u} \cdot \nabla \theta, \theta_t \rangle, \quad (2.3.5)$$

where the indefinite SUPG term (i.e. the last term) is kept small by a suitable choice of τ . Note that since all test functions were modified to include an upwind term, the resulting weak equation (2.3.4) is still clearly consistent, in the sense that an exact solution to the continuous equation (2.3.1) also solves the weak equation.

The upwinded advection equation (2.3.4) can be used for fully continuous spaces \mathbb{V}_{θ} , as is the case for our choice of buoyancy space for the thermal shallow water equations. For spaces that are not fully continuous, such as the Charney-Phillips type finite element space defined above, further care needs to be taken for the discontinuous components. In our case, we follow [20], and apply the standard DG upwinding scheme [13] in the horizontal (i.e. discontinuous) direction, and restrict

the SUPG setup to the vertical direction. To this end, we first integrate the weak form (2.3.2) by parts and arrive at

$$\langle \gamma, \theta_t \rangle - \langle \nabla \cdot (\mathbf{u}\gamma), \theta \rangle + \int_{\Gamma_v} \llbracket \mathbf{u}\gamma \rrbracket \tilde{\theta} dS = 0 \quad \forall \gamma \in \mathbb{V}_\theta, \quad (2.3.6)$$

where Γ_v denotes the set of all vertical interior facets of the underlying mesh. The jump operator $\llbracket \cdot \rrbracket$ (for vectors \mathbf{v} and scalars ψ , respectively) and upwind value $\tilde{\theta}$ are defined by

$$\begin{aligned} \llbracket \mathbf{v} \rrbracket &= \mathbf{v}^+ \cdot \mathbf{n}^+ + \mathbf{v}^- \cdot \mathbf{n}^-, \\ \llbracket \psi \rrbracket &= \psi^+ - \psi^-, \end{aligned} \quad \tilde{\theta} = \begin{cases} \theta^+ & \text{if } \mathbf{u} \cdot \mathbf{n}^+ < 0, \\ \theta^- & \text{otherwise,} \end{cases} \quad (2.3.7)$$

noting that the two sides of each mesh facet are arbitrarily denoted by $+$ and $-$ (and hence $\mathbf{n}^+ = -\mathbf{n}^-$). Before incorporating the upwind modification (2.3.3) to the test functions in (2.3.6), we need to integrate by parts again to avoid applying the differential operator ∇ to the upwinded part $\tau \mathbf{u} \cdot \nabla \gamma$, as the double differentiation may not be well-defined for $\gamma \in \mathbb{V}_\theta$. Further, we restrict the SUPG scheme to the vertical direction by using modified test functions of form

$$\gamma \rightarrow \gamma + \tau(\mathbf{k} \cdot \mathbf{u})(\mathbf{k} \cdot \nabla \gamma) =: \gamma_{(\mathbf{k} \cdot \mathbf{u})\mathbf{k}}, \quad (2.3.8)$$

for vertical unit vector \mathbf{k} . The resulting, fully upwinded advection equation is then given by

$$\langle \gamma_{(\mathbf{k} \cdot \mathbf{u})\mathbf{k}}, \theta_t \rangle + \langle \gamma_{(\mathbf{k} \cdot \mathbf{u})\mathbf{k}}, \mathbf{u} \cdot \nabla \theta \rangle + \int_{\Gamma_v} (\llbracket \mathbf{u}\gamma_{(\mathbf{k} \cdot \mathbf{u})\mathbf{k}} \rrbracket \tilde{\theta} - \llbracket \mathbf{u}\gamma_{(\mathbf{k} \cdot \mathbf{u})\mathbf{k}} \theta \rrbracket) dS = 0 \quad \forall \gamma \in \mathbb{V}_\theta. \quad (2.3.9)$$

In the next section, we will incorporate the stabilised advection schemes (2.3.4) and (2.3.9) in the energy conserving bracket (2.1.2) - (2.1.3). To simplify notation, we write the upwinded test functions (2.3.3) and (2.3.8) as well as advection terms (2.3.4) and (2.3.9) as operators given in the definition below.

Definition 1 *The SUPG contribution to $\gamma \in \mathbb{V}_\theta$ is given by*

$$\tilde{\gamma}_{\mathbf{u}} := \begin{cases} \tau \mathbf{u} \cdot \nabla \gamma & \text{CG type } \mathbb{V}_\theta, \\ \tau(\mathbf{k} \cdot \mathbf{u})(\mathbf{k} \cdot \nabla \gamma) & \text{CP type } \mathbb{V}_\theta. \end{cases} \quad (2.3.10)$$

Further, the discrete thermal field transport operator is given by

$$L_{\mathbf{v}}^\theta(\theta; \gamma_{\mathbf{u}}) = \begin{cases} \langle \gamma + \tilde{\gamma}_{\mathbf{u}}, \mathbf{v} \cdot \nabla \theta \rangle & \text{CG type } \mathbb{V}_\theta, \\ \langle \gamma + \tilde{\gamma}_{\mathbf{u}}, \mathbf{v} \cdot \nabla \theta \rangle + \int_{\Gamma_v} (\llbracket \mathbf{v}(\gamma + \tilde{\gamma}_{\mathbf{u}}) \rrbracket \tilde{\theta} - \llbracket \mathbf{v}(\gamma + \tilde{\gamma}_{\mathbf{u}}) \theta \rrbracket) dS & \text{CP type } \mathbb{V}_\theta. \end{cases} \quad (2.3.11)$$

Using this definition, we can rewrite the advection equations (2.3.4) and (2.3.9) as a single equation of form

$$\langle \gamma + \tilde{\gamma}_{\mathbf{u}}, \theta_t \rangle + L_{\mathbf{u}}^\theta(\theta; \gamma_{\mathbf{u}}) = 0 \quad \forall \gamma \in \mathbb{V}_\theta. \quad (2.3.12)$$

Finally, we note that the lowered \mathbf{u} at L corresponds to the advecting velocity, while the lowered \mathbf{u} at γ corresponds to the velocity used for upwinding. Depending on the time discretisation, we will find that these may be distinct in the almost Poisson bracket setup.

2.4 SUPG upwinding in the discretised bracket

It remains to incorporate SUPG upwinding, as described in Section 2.3, into the discretised almost Poisson bracket. Without upwinding, the bracket is given by (2.1.2) - (2.1.3), such that $q \in \mathbb{V}_q$, $\rho \in \mathbb{V}_\rho$, $\theta \in \mathbb{V}_\theta$, and the variations are functions of the corresponding finite element spaces. We aim to replace the corresponding thermal field advection equation (2.2.7) by the SUPG version (2.3.12), i.e.

$$\langle \gamma, \theta_t \rangle + \langle \gamma, \frac{1}{\rho} \frac{\delta H}{\delta \mathbf{u}} \cdot \nabla \theta \rangle = 0 \quad \rightarrow \quad \langle \gamma + \tilde{\gamma}_{\mathbf{u}}, \theta_t \rangle + L_{\frac{\delta H}{\delta \mathbf{u}}/\rho}^\theta(\theta; \gamma_{\mathbf{u}}) = 0, \quad (2.4.1)$$

where as for the non-upwinded version, we anticipate an advecting velocity of form $\frac{\delta H}{\delta \mathbf{u}}/\rho$ when upwinding is included. Note that in the Poisson system (2.1.1), the time derivative term $\langle \gamma, \theta_t \rangle$ corresponds to $\frac{dF}{dt}$, while the advection term is derived from the bracket $\{F, H\}$. Considering the upwinded equation, we find that choosing

$$F = \langle \gamma + \tilde{\gamma}_{\mathbf{u}}, \theta \rangle \quad (2.4.2)$$

in the Poisson system is impractical, since then the time derivative of F will include a time derivative in the upwinding velocity \mathbf{u} . To avoid this, we move the corresponding upwinding part to the right-hand side:

$$\langle \gamma, \theta_t \rangle = -L_{\frac{\delta H}{\delta \rho}/\mathbf{u}}^\theta(\theta; \gamma_{\mathbf{u}}) - \langle \tilde{\gamma}_{\mathbf{u}}, \theta_t \rangle, \quad (2.4.3)$$

that is we will consider the upwind part $\tilde{\gamma}_{\mathbf{u}}$ of the time derivative term as part of the Poisson bracket. Including this term in the bracket, however, leads to further complications. First, a corresponding antisymmetric term needs to be added, which will appear in the momentum equation's forcing part. Second, in view of the energy conserving time integration scheme to be used below, the bracket should be independent of time derivatives. This means that θ_t in the bracket should be replaced by another, time-derivative free term. Considering the upwinded equation (2.4.1), we find that θ_t depends on the advection operator L as well as the upwinded test function contribution $\tilde{\gamma}_{\mathbf{u}}$, motivating Definition 2 below.

Definition 2 *The thermal field advection operator $\theta^a: \mathbb{V}_{\mathbf{u}} \rightarrow \mathbb{V}_\theta$ is given by*

$$\langle \gamma, \theta^a(\mathbf{w}) \rangle = -L_{\mathbf{w}/\rho}^\theta(\theta; \gamma_{\mathbf{u}}) \quad \forall \gamma \in \mathbb{V}_\theta. \quad (2.4.4)$$

Further, the SUPG recovery operator $\mathbb{S}_{\mathbf{u}}: \mathbb{V}_\theta \rightarrow \mathbb{V}_\theta$ is given by

$$\langle \gamma, \mathbb{S}_{\mathbf{u}}(\tau) \rangle = \langle \gamma + \tilde{\gamma}_{\mathbf{u}}, \tau \rangle \quad \forall \gamma \in \mathbb{V}_\theta. \quad (2.4.5)$$

Note that both θ^a and $\mathbb{S}_{\mathbf{u}}$ implicitly also depend on the state $\mathbf{z} = (\mathbf{u}, \rho, \theta)$. Using these two operators, we can rewrite the upwinded thermal field advection equation (2.4.1) as

$$\langle \gamma, \mathbb{S}_{\mathbf{u}}(\theta_t) \rangle = \langle \gamma, \theta^a\left(\frac{\delta H}{\delta \mathbf{u}}\right) \rangle \quad \forall \gamma \in \mathbb{V}_\theta, \quad (2.4.6)$$

for any test function γ . Since both θ^a and $\mathbb{S}_{\mathbf{u}}$ map into \mathbb{V}_θ , this implies $\theta^a = \mathbb{S}_{\mathbf{u}}(\theta_t)$ point-wise, and therefore $\theta_t = \mathbb{S}_{\mathbf{u}}^{-1}(\theta^a)$, provided $\mathbb{S}_{\mathbf{u}}^{-1}$ exists. This motivates a modified, upwinded θ variation part of the bracket according to

$$+ \langle \frac{1}{\rho} \frac{\delta H}{\delta \theta} \nabla \theta, \frac{\delta F}{\delta \mathbf{u}} \rangle \quad \rightarrow \quad + L_{\frac{\delta F}{\delta \mathbf{u}}/\rho}^\theta\left(\theta; \left(\frac{\delta H}{\delta \theta}\right)_{\mathbf{u}}\right) + \langle \left(\frac{\delta H}{\delta \theta}\right)_{\mathbf{u}}, \mathbb{S}_{\mathbf{u}}^{-1}\left(\theta^a\left(\frac{\delta F}{\delta \mathbf{u}}\right)\right) \rangle \quad (2.4.7)$$

$$- \langle \frac{1}{\rho} \frac{\delta F}{\delta \theta} \nabla \theta, \frac{\delta H}{\delta \mathbf{u}} \rangle \quad \rightarrow \quad - L_{\frac{\delta H}{\delta \mathbf{u}}/\rho}^\theta\left(\theta; \left(\frac{\delta F}{\delta \theta}\right)_{\mathbf{u}}\right) - \langle \left(\frac{\delta F}{\delta \theta}\right)_{\mathbf{u}}, \mathbb{S}_{\mathbf{u}}^{-1}\left(\theta^a\left(\frac{\delta H}{\delta \mathbf{u}}\right)\right) \rangle, \quad (2.4.8)$$

where (2.4.8) corresponds to the thermal field advection equation, while (2.4.7) does to the corresponding antisymmetric bracket term, which appears as a forcing term in the momentum equation. Note that L^θ is bilinear in F and H (considering its definition (2.3.11)) and further that since both θ^a and $\mathbb{S}_{\mathbf{u}}$ are linear, the corresponding upwind contribution bracket term is also bilinear. Since (2.4.7) and (2.4.8) form an antisymmetric pair by construction, we therefore find that the modified, upwinded bracket given in Definition 3 below is still an antisymmetric bilinear form. In Proposition 1, we confirm that this setup does indeed lead to an SUPG equation of form (2.4.1).

Definition 3 *The thermal field upwinded almost Poisson bracket $\{F, H\}$ is given by*

$$-\langle \frac{\delta F}{\delta \mathbf{u}}, \mathbf{q} \times \frac{\delta H}{\delta \mathbf{u}} \rangle + \langle \frac{\delta H}{\delta \rho}, \nabla \cdot \frac{\delta F}{\delta \mathbf{u}} \rangle + L_{\frac{\delta F}{\delta \mathbf{u}}/\rho}^\theta \left(\theta; \left(\frac{\delta H}{\delta \theta} \right)_{\mathbf{u}} \right) + \langle \left(\frac{\delta H}{\delta \theta} \right)_{\mathbf{u}}, \mathbb{S}_{\mathbf{u}}^{-1} \left(\theta^a \left(\frac{\delta F}{\delta \mathbf{u}} \right) \right) \rangle \quad (2.4.9)$$

$$- \langle \frac{\delta F}{\delta \rho}, \nabla \cdot \frac{\delta H}{\delta \mathbf{u}} \rangle - L_{\frac{\delta H}{\delta \mathbf{u}}/\rho}^\theta \left(\theta; \left(\frac{\delta F}{\delta \theta} \right)_{\mathbf{u}} \right) - \langle \left(\frac{\delta F}{\delta \theta} \right)_{\mathbf{u}}, \mathbb{S}_{\mathbf{u}}^{-1} \left(\theta^a \left(\frac{\delta H}{\delta \mathbf{u}} \right) \right) \rangle, \quad (2.4.10)$$

with operators L^θ , θ^a and \mathbb{S} given by Definitions 1 and 2.

Proposition 1 *Consider the space discretised almost Poisson bracket given by Definition 3. Then the thermal field transport equation based on the Poisson system (2.1.1) with this bracket is given by*

$$\langle \gamma + \tilde{\gamma}_{\mathbf{u}}, \theta_t \rangle + L_{\frac{\delta H}{\delta \mathbf{u}}/\rho}^\theta(\theta; \gamma_{\mathbf{u}}) = 0 \quad \forall \gamma \in \mathbb{V}_\theta. \quad (2.4.11)$$

Proof. *We test the upwinded bracket using the usual functional of form $F = \langle \gamma, \theta \rangle$. In this case, as before all parts of the bracket except for the ones corresponding to temperature advection (i.e. (2.4.8)) are zero, and we are left with*

$$\frac{dF}{dt} = \langle \gamma, \theta_t \rangle = -L_{\frac{\delta H}{\delta \mathbf{u}}/\rho}^\theta(\theta; \gamma_{\mathbf{u}}) - \langle \tilde{\gamma}_{\mathbf{u}}, \mathbb{S}_{\mathbf{u}}^{-1} \left(\theta^a \left(\frac{\delta H}{\delta \mathbf{u}} \right) \right) \rangle. \quad (2.4.12)$$

By definition of θ^a , the advection operator part of the right-hand side is equal to $\langle \gamma, \theta^a \left(\frac{\delta H}{\delta \mathbf{u}} \right) \rangle$, which in turn can be expressed using \mathbb{S} as

$$\langle \gamma + \tilde{\gamma}_{\mathbf{u}}, \mathbb{S}_{\mathbf{u}}^{-1} \left(\theta^a \left(\frac{\delta H}{\delta \mathbf{u}} \right) \right) \rangle. \quad (2.4.13)$$

We can then cancel with the upwind contribution term (i.e. the last term in (2.4.12)), so that

$$\langle \gamma, \theta_t \rangle = \langle \gamma, \mathbb{S}_{\mathbf{u}}^{-1} \left(\theta^a \left(\frac{\delta H}{\delta \mathbf{u}} \right) \right) \rangle, \quad (2.4.14)$$

which holds for any γ . Hence, the $\mathbb{S}_{\mathbf{u}}^{-1} \theta^a$ term is identically equal to θ_t , and we may replace it in (2.4.12). Moving the upwind contribution term and the advection operator to the left-hand side then gives the required upwinded form. \square

The second implication of including a θ_t term in the bracket lies in the corresponding antisymmetric term (i.e. the second term in (2.4.7)), given by

$$\langle \left(\frac{\delta H}{\delta \theta} \right)_{\mathbf{u}}, \mathbb{S}_{\mathbf{u}}^{-1} \left(\theta^a \left(\frac{\delta F}{\delta \mathbf{u}} \right) \right) \rangle. \quad (2.4.15)$$

The test function $\frac{\delta F}{\delta \mathbf{u}}$ appears as an argument of $\mathbb{S}_{\mathbf{u}}^{-1} \theta^a$, which we would be required to solve for for every test function in the variational solver for the velocity. To avoid this, we use the transpose of $\mathbb{S}_{\mathbf{u}}^{-1} \theta^a$, allowing us to move the operator away from the test function.

Proposition 2 Consider the space discretised almost Poisson bracket given by Definition 3. Then the momentum equation based on the Poisson system (2.1.1) with this bracket is given by

$$\langle \mathbf{w}, \mathbf{u}_t \rangle + \langle \mathbf{w}, \mathbf{q} \times \frac{\delta H}{\delta \mathbf{u}} \rangle + \langle \frac{\delta H}{\delta \rho}, \nabla \cdot \mathbf{w} \rangle + L_{\mathbf{w}/\rho}^\theta \left(\theta; \left(\frac{\delta H}{\delta \theta} \right)_{\mathbf{u}} \right) + \langle \mathbf{s} \left(\frac{\delta \widetilde{H}}{\delta \theta} \right), \mathbf{w} \rangle = 0 \quad \forall \mathbf{w} \in \mathbb{V}_u, \quad (2.4.16)$$

where $\mathbf{s} \in \mathbb{V}_u$ is given by

$$\langle \mathbf{s}, \mathbf{v} \rangle = -L_{\mathbf{v}/\rho}^\theta(\theta; \sigma_{\mathbf{u}}) \quad \forall \mathbf{v} \in \mathbb{V}_u, \quad (2.4.17)$$

for $\sigma \in \mathbb{V}_\theta$ such that

$$\langle \eta, \sigma_{\mathbf{u}} \rangle = \langle \eta, \left(\frac{\delta \widetilde{H}}{\delta \theta} \right)_{\mathbf{u}} \rangle \quad \forall \eta \in \mathbb{V}_\theta. \quad (2.4.18)$$

Proof. The first three terms (excluding the time derivative term) follow directly from the bracket, using $F = \langle \mathbf{w}, \mathbf{u} \rangle$ in the Poisson system. To obtain the last term, we evaluate the the corresponding bracket term (2.4.15) as

$$\langle (\theta^a)^*(\mathbb{S}_{\mathbf{u}}^{-1})^* \left(\left(\frac{\delta \widetilde{H}}{\delta \theta} \right)_{\mathbf{u}} \right), \frac{\delta F}{\delta \mathbf{u}} \rangle, \quad (2.4.19)$$

for transpose operator $*$. First, for θ^a , we find directly that its transpose $(\theta^a)^*: \mathbb{V}_\theta \rightarrow \mathbb{V}_u$ is given by

$$\langle (\theta^a)^*(\gamma), \mathbf{v} \rangle = -L_{\mathbf{v}/\rho}^\theta(\theta; \gamma_{\mathbf{u}}) \quad \forall \mathbf{v} \in \mathbb{V}_u, \quad (2.4.20)$$

while for the upwind operator we note that $(\mathbb{S}_{\mathbf{u}}^{-1})^* = (\mathbb{S}_{\mathbf{u}}^*)^{-1}$, with $\mathbb{S}_{\mathbf{u}}^*$ clearly following from the definition of $\mathbb{S}_{\mathbf{u}}$ as

$$\mathbb{S}_{\mathbf{u}}^*(\gamma) = P_{\mathbb{V}_\theta}(\gamma + \tilde{\gamma}_{\mathbf{u}}). \quad (2.4.21)$$

To find the inverse, we search for a γ such that, given “an upwinded function” $\chi \in \mathbb{V}_\theta$,

$$\langle \eta, \chi \rangle = \langle \eta, \gamma_{\mathbf{u}} \rangle \quad \forall \eta \in \mathbb{V}_\theta. \quad (2.4.22)$$

Finally, we solve this for γ with

$$\chi = \left(\frac{\delta \widetilde{H}}{\delta \theta} \right)_{\mathbf{u}}, \quad (2.4.23)$$

which yields σ as defined above. \mathbf{s} then follows applying (2.4.20) on σ , as required. \square

Using Propositions 1 and 2, we obtain from the θ -upwinded discretised bracket in Definition 3 a system of equations of form

$$\langle \mathbf{w}, \mathbf{u}_t \rangle + \langle \mathbf{w}, \mathbf{q} \times \frac{\delta H}{\delta \mathbf{u}} \rangle + \langle \frac{\delta H}{\delta \rho}, \nabla \cdot \mathbf{w} \rangle + L_{\mathbf{w}/\rho}^\theta \left(\theta; \left(\frac{\delta H}{\delta \theta} \right)_{\mathbf{u}} \right) + \langle \mathbf{s} \left(\frac{\delta \widetilde{H}}{\delta \theta} \right), \mathbf{w} \rangle = 0 \quad \forall \mathbf{w} \in \mathbb{V}_u, \quad (2.4.24)$$

$$\langle \phi, \rho_t \rangle + \langle \phi, \nabla \cdot \frac{\delta H}{\delta \mathbf{u}} \rangle = 0 \quad \forall \phi \in \mathbb{V}_\rho, \quad (2.4.25)$$

$$\langle \gamma + \tilde{\gamma}_{\mathbf{u}}, \theta_t \rangle + L_{\frac{\delta H}{\delta \mathbf{u}}/\rho}^\theta(\theta; \gamma_{\mathbf{u}}) = 0 \quad \forall \gamma \in \mathbb{V}_\theta. \quad (2.4.26)$$

Finally, in a similar fashion to the proofs above, we find that the Poisson system can be recovered from these equations from the chain rule for F as in (2.1.12). Since the θ -upwinded discretised bracket is antisymmetric, we therefore find that equations (2.4.24) - (2.4.26) are still energy conserving.

Remark 1 To also incorporate energy conserving upwinding schemes for \mathbf{u} and ρ in the equation set (2.4.24) - (2.4.26), we can use the framework provided in [26], where a bracket for the rotating shallow water equations was considered. The bracket is identical to the one introduced above, up to excluding the two thermal terms (i.e. setting $\frac{\delta H}{\delta \theta} = 0$ in (2.4.9) and $\frac{\delta F}{\delta \theta} = 0$ in (2.4.10)), and we can directly apply the upwinding schemes here. The shallow water upwinded bracket is given by

$$\{F, H\} := \langle \nabla^\perp(\rho \mathbb{U}(\rho, \frac{\delta F}{\delta \mathbf{u}}) \cdot \mathbb{U}(\rho, \frac{\delta H}{\delta \mathbf{u}})^\perp), \mathbf{u} \rangle - \int_\Gamma \llbracket \rho \mathbb{U}(\rho, \frac{\delta F}{\delta \mathbf{u}}) \cdot \mathbb{U}(\rho, \frac{\delta H}{\delta \mathbf{u}})^\perp \rrbracket \mathbf{n}^\perp \cdot \tilde{\mathbf{u}} dS \quad (2.4.27)$$

$$- \langle \rho \mathbb{U}(\rho, \frac{\delta F}{\delta \mathbf{u}}), \nabla \frac{\delta H}{\delta \rho} \rangle + \int_\Gamma \llbracket \frac{\delta H}{\delta \rho} \mathbb{U}(\rho, \frac{\delta F}{\delta \mathbf{u}}) \rrbracket \tilde{\rho} dS - \langle \rho \mathbb{U}(\rho, \frac{\delta F}{\delta \mathbf{u}}), f \mathbb{U}(\rho, \frac{\delta H}{\delta \mathbf{u}})^\perp \rangle \quad (2.4.28)$$

$$+ \langle \rho \mathbb{U}(\rho, \frac{\delta H}{\delta \mathbf{u}}), \nabla \frac{\delta F}{\delta \rho} \rangle - \int_\Gamma \llbracket \frac{\delta F}{\delta \rho} \mathbb{U}(\rho, \frac{\delta H}{\delta \mathbf{u}}) \rrbracket \tilde{\rho} dS, \quad (2.4.29)$$

where (2.4.27) corresponds to velocity advection, (2.4.28) to the forcing terms in the momentum equation, and (2.4.29) to density advection. For the purpose of density upwinding, a velocity recovery operator \mathbb{U} of form

$$\mathbb{U}(D, \mathbf{m}) : \mathbb{V}_\rho \times \mathbb{V}_u \longrightarrow \mathbb{V}_u \quad \text{such that} \quad \langle D\mathbf{v}, \mathbb{U} \rangle = \langle \mathbf{v}, \mathbf{m} \rangle \quad \forall \mathbf{v} \in \mathbb{V}_u, \quad (2.4.30)$$

was introduced (for details, see [26]). Note that \mathbb{U} corresponds to a discrete division by ρ , and recalling that $\frac{\delta H}{\delta \mathbf{u}}$ is given by the discrete flux $P_{\mathbb{V}_u}(\rho \mathbf{u})$, we find that $\mathbb{U}(\rho, \frac{\delta H}{\delta \mathbf{u}}) \in \mathbb{V}_u$ corresponds to the advecting velocity for \mathbf{u} and ρ advection. The bracket then leads to an upwinded density equation of form

$$\langle \phi, \rho_t \rangle = \langle \rho \mathbb{U}(\rho, \frac{\delta H}{\delta \mathbf{u}}), \nabla \phi \rangle - \int_\Gamma \llbracket \phi \mathbb{U}(\rho, \frac{\delta H}{\delta \mathbf{u}}) \rrbracket \tilde{\rho} dS \quad \forall \phi \in \mathbb{V}_\rho, \quad (2.4.31)$$

which corresponds to the standard DG upwind scheme. For the velocity equation, we obtain

$$\langle \mathbf{w}, \mathbf{u}_t \rangle = \langle \nabla^\perp(\rho \mathbb{U}(\rho, \mathbf{w}) \cdot \mathbb{U}(\rho, \frac{\delta H}{\delta \mathbf{u}})^\perp), \mathbf{u} \rangle - \int_\Gamma \llbracket \rho \mathbb{U}(\rho, \mathbf{w}) \cdot \mathbb{U}(\rho, \frac{\delta H}{\delta \mathbf{u}})^\perp \rrbracket \mathbf{n}^\perp \cdot \tilde{\mathbf{u}} dS \quad (2.4.32)$$

$$- \langle \rho \mathbb{U}(\rho, \mathbf{w}), f \mathbb{U}(\rho, \frac{\delta H}{\delta \mathbf{u}})^\perp \rangle \quad (2.4.33)$$

$$- \langle \rho \mathbb{U}(\rho, \mathbf{w}), \nabla \frac{\delta H}{\delta \rho} \rangle + \int_\Gamma \llbracket \frac{\delta H}{\delta \rho} \mathbb{U}(\rho, \mathbf{w}) \rrbracket \tilde{\rho} dS \quad \forall \mathbf{w} \in \mathbb{V}_u, \quad (2.4.34)$$

where upwinding was applied to the rotational velocity advection part, given by $(\nabla^\perp \cdot \mathbf{u}) \mathbf{u}^\perp$. Note that the velocity recovery operator is applied to all test functions on the right hand side of the velocity equation. For a consistent use of test functions, when extending this bracket to the thermal case, we then also apply this operator to the test functions of the corresponding thermal bracket term (2.4.7). To maintain antisymmetry, we then also need to apply it in (2.4.8), and we arrive at a fully upwinded bracket given by (2.4.27) - (2.4.29), together with

$$+ L_{\mathbb{U}(\rho, \frac{\delta F}{\delta \mathbf{u}})}^\theta \left(\theta; \left(\frac{\delta H}{\delta \theta} \right)_\mathbf{u} \right) + \left\langle \left(\frac{\delta H}{\delta \theta} \right)_\mathbf{u}, \mathbb{S}_\mathbf{u}^{-1} \left(\theta^a \left(\mathbb{U}(\rho, \frac{\delta F}{\delta \mathbf{u}}) \right) \right) \right\rangle \quad (2.4.35)$$

$$- L_{\mathbb{U}(\rho, \frac{\delta H}{\delta \mathbf{u}})}^\theta \left(\theta; \left(\frac{\delta F}{\delta \theta} \right)_\mathbf{u} \right) - \left\langle \left(\frac{\delta F}{\delta \theta} \right)_\mathbf{u}, \mathbb{S}_\mathbf{u}^{-1} \left(\theta^a \left(\mathbb{U}(\rho, \frac{\delta H}{\delta \mathbf{u}}) \right) \right) \right\rangle, \quad (2.4.36)$$

and θ^a now defined by

$$\langle \gamma, \theta^a(\mathbf{v}) \rangle = -L_\mathbf{v}^\theta(\theta; \gamma_\mathbf{u}) \quad \forall \gamma \in \mathbb{V}_\theta. \quad (2.4.37)$$

The flux recovered velocity $\mathbb{U}(\rho, \frac{\delta H}{\delta \mathbf{u}})$ then also serves as the advecting velocity for the thermal field transport equation, given by

$$\langle \gamma + \tilde{\gamma}_{\mathbf{u}}, \theta_t \rangle + L_{\mathbb{U}(\rho, \frac{\delta H}{\delta \mathbf{u}})}^\theta(\theta; \gamma_{\mathbf{u}}) \quad \forall \gamma \in \mathbb{V}_\theta. \quad (2.4.38)$$

Finally, we note that the underlying 2D velocity advection scheme and Coriolis term in (2.4.27) and (2.4.28) above can be extended readily to the three-dimensional case [20], which in our case leads to

$$\langle \nabla \times (\rho \mathbb{U}(\rho, \frac{\delta F}{\delta \mathbf{u}}) \times \mathbb{U}(\rho, \frac{\delta H}{\delta \mathbf{u}})), \mathbf{u} \rangle - \int_\Gamma \{ \{ \mathbf{n} \times (\rho \mathbb{U}(\rho, \frac{\delta F}{\delta \mathbf{u}}) \times \mathbb{U}(\rho, \frac{\delta H}{\delta \mathbf{u}})) \} \} \cdot \tilde{\mathbf{u}} \, dS \quad (2.4.39)$$

$$- \langle \rho \mathbb{U}(\rho, \frac{\delta F}{\delta \mathbf{u}}), 2\boldsymbol{\Omega} \times \mathbb{U}(\rho, \frac{\delta H}{\delta \mathbf{u}}) \rangle, \quad (2.4.40)$$

where

$$\{ \{ \mathbf{n} \times \mathbf{w} \} \} = \mathbf{n}^+ \times \mathbf{w}^+ + \mathbf{n}^- \times \mathbf{w}^-. \quad (2.4.41)$$

3 Numerical results

In this section, we confirm numerically the upwind stabilised and energy conserving properties of the newly introduced almost Poisson bracket (2.4.9) - (2.4.10). First, we review the energy conserving time discretisation used for this purpose, as well as the resulting non-linear set of equations. Next, we discuss the operational applicability of the bracket, including simplifications in view of computational costs and the extension to a fully upwinded bracket. Finally, we present test cases, consisting of a perturbed thermogeostrophic balance scenario for the thermal shallow water equations, as well as a cold and hot air bubble scenario for the Euler equations.

3.1 Time discretisation and nonlinear system

To confirm the energy conserving property of the space discretised equations (2.4.24) - (2.4.26), we apply an energy conserving time discretisation, thus expecting energy conservation up to machine precision. It is given by a Poisson integrator as introduced in [6], and can be applied to the framework used here as detailed in [26]. For the prognostic fields $\mathbf{z} = (\mathbf{u}, \rho, \theta)$, we have

$$\mathbf{z}^{n+1} = \mathbf{z}^n + \Delta t J \left(\frac{\mathbf{z}^{n+1} + \mathbf{z}^n}{2} \right) \left(\overline{\frac{\delta H}{\delta \mathbf{u}}}, \overline{\frac{\delta H}{\delta \rho}}, \overline{\frac{\delta H}{\delta \theta}} \right)^T, \quad (3.1.1)$$

where the skew symmetric transformation J is related to the almost Poisson bracket via

$$\{F, H\} = \left\langle \frac{\delta F}{\delta \mathbf{z}}, J(\mathbf{z}) \frac{\delta H}{\delta \mathbf{z}} \right\rangle, \quad (3.1.2)$$

and the time averaged Hamiltonians are given by

$$\overline{\frac{\delta H}{\delta \mathbf{u}}} := \int_0^1 \frac{\delta}{\delta \mathbf{u}} H(\mathbf{z}^n + s(\mathbf{z}^{n+1} - \mathbf{z}^n)) ds, \quad (3.1.3)$$

and similarly for the variations in ρ and θ . The expressions can be integrated exactly for the thermal shallow water Hamiltonian, leading to

$$\overline{\frac{\delta H}{\delta \mathbf{u}}} = \frac{1}{3} P_{\mathbb{V}_u} (\rho^n \mathbf{u}^n + \frac{1}{2} \rho^n \mathbf{u}^{n+1} + \frac{1}{2} \rho^{n+1} \mathbf{u}^n + \rho^{n+1} \mathbf{u}^{n+1}), \quad (3.1.4)$$

and similarly for the other two variations. However, for the Euler Hamiltonian, we find that the internal energy is a non-polynomial function in ρ , θ , thus requiring an approximate integration of

(3.1.3) for the variations in ρ and θ . For the numerical results below, a fourth order Gaussian quadrature was used.

The resulting nonlinear system of equations is given by

$$\langle \mathbf{w}, \mathbf{u}^{n+1} - \mathbf{u}^n \rangle + \Delta t \left(\langle \mathbf{w}, \bar{\mathbf{q}} \times \frac{\overline{\delta H}}{\delta \mathbf{u}} \rangle - \langle \frac{\overline{\delta H}}{\delta \rho}, \nabla \cdot \mathbf{w} \rangle \right) \quad (3.1.5)$$

$$- L_{\mathbf{w}/\bar{\rho}}^\theta \left(\bar{\theta}; \left(\frac{\overline{\delta H}}{\delta \theta} \right)_{\bar{\mathbf{u}}} \right) - \langle \mathbf{s} \left(\frac{\overline{\delta H}}{\delta \theta} \right), \mathbf{w} \rangle = 0 \quad \forall \mathbf{w} \in \mathbb{V}_u, \quad (3.1.6)$$

$$\langle \phi, \rho^{n+1} - \rho^n \rangle + \Delta t \langle \phi, \nabla \cdot \frac{\overline{\delta H}}{\delta \mathbf{u}} \rangle = 0 \quad \forall \phi \in \mathbb{V}_\rho, \quad (3.1.7)$$

$$\langle \gamma_{\bar{\mathbf{u}}}, \theta^{n+1} - \theta^n \rangle + \Delta t L_{\frac{\overline{\delta H}}{\delta \mathbf{u}}/\bar{\rho}}^\theta (\bar{\theta}; \gamma_{\bar{\mathbf{u}}}) = 0 \quad \forall \gamma \in \mathbb{V}_\theta, \quad (3.1.8)$$

for midpoint time average $\bar{\rho} = (\rho^n + \rho^{n+1})/2$, and similar for $\bar{\mathbf{u}}$ and $\bar{\mathbf{q}}$, with \mathbf{q}^n and \mathbf{q}^{n+1} given by the diagnostic scalar vorticity relation (2.2.8), using the prognostic fields at time levels n and $n+1$, respectively. Note that all occurrences of the state \mathbf{z} in L^θ and \mathbf{s} are also discretised at the half-time level. Further, we remark that the derivation of the fully discretised thermal field equation (3.1.8) follows the proof of Proposition 1 in a time discretised form, with θ_t replaced by $(\theta^{n+1} - \theta^n)/\Delta t$.

To solve for \mathbf{z}^{n+1} , given the fully discretised residual $\mathbf{R}(\mathbf{z}^{n+1})$ above (left-hand sides of (3.1.5) - (3.1.8)), we apply the same procedure as detailed in [26] and revert to a Picard iteration scheme. For update $\delta \mathbf{z} = \mathbf{z}^{n+1,k+1} - \mathbf{z}^{n+1,k}$ with unknown next time step estimate $\mathbf{z}^{n+1,k+1}$, we set

$$\frac{\delta \mathbf{R}'}{\delta \mathbf{z}}(\delta \mathbf{z}) = -\mathbf{R}(\mathbf{z}^{n+1,k}), \quad (3.1.9)$$

and $\mathbf{z}^{n+1,0} = \mathbf{z}^n$. The left hand side corresponds to the Jacobian of a linearised version of \mathbf{R} without Hamiltonian projections, and is given by

$$\frac{\delta \mathbf{R}'}{\delta \mathbf{z}}(\delta \mathbf{z}) = \begin{pmatrix} \langle \delta \mathbf{u}, \mathbf{w} \rangle + \frac{\Delta t}{2} \left(2\bar{\boldsymbol{\Omega}} \times \delta \mathbf{u}, \mathbf{w} \right) - \langle g\delta \rho + c_p(\bar{\bar{\theta}}\delta \pi + \delta \theta \bar{\bar{\pi}}), \nabla \cdot \mathbf{w} \rangle + c_p \langle \bar{\bar{\pi}} \nabla \delta \theta, \mathbf{w} \rangle \\ \langle \delta \rho, \phi \rangle + \frac{\Delta t}{2} \langle \bar{\rho} \nabla \cdot \delta \mathbf{u}, \phi \rangle \\ \langle \delta \theta, \gamma \rangle \end{pmatrix}, \quad (3.1.10)$$

where double-barred entries correspond to background fields, with $\bar{\bar{\pi}} = \pi(\bar{\bar{\rho}}, \bar{\bar{\theta}})$, $\bar{\mathbf{u}} = \mathbf{0}$, and $\delta \pi = \frac{\partial \pi}{\partial \bar{\rho}}(\bar{\bar{\rho}}, \bar{\bar{\theta}})\delta \rho + \frac{\partial \pi}{\partial \bar{\theta}}(\bar{\bar{\rho}}, \bar{\bar{\theta}})\delta \theta$. Note that in view of the test cases to follow, we assumed the background thermal field to be constant (equal to g for the thermal shallow water equations, and an isentropic background potential temperature for the Euler equations). This leads to a vanishing $\nabla \bar{\bar{\theta}}$ term in the velocity and thermal field equation, respectively, thus uncoupling the latter from the density and velocity equations. Given the right-hand side $-\mathbf{R}(\mathbf{z}^{n+1,k})$ we can then first solve for $\delta \theta$, followed by a mixed solve for the density and velocity updates. Note that since this paper focuses on the underlying space discretisation, the nonlinear solve procedure is kept simple. The discretisation can in principle be applied equally to fully three-dimensional problems and scenarios with a non-constant potential background temperature (by approximately eliminating $\delta \theta$ in the linearised momentum equation). A suitable nonlinear solver strategy for this case can be found in [2].

The mesh, finite element discretisation, and solver were implemented using the automated finite element toolkit Firedrake¹ [21], with a hybridised solver (see e.g. [23]) used to solve for the mixed system in $(\delta \mathbf{u}, \delta \rho)$.

¹for further details, see [3, 11, 12, 15] or <http://firedrakeproject.org>

3.2 Fully upwinded, approximately energy conserving formulation

While both the space and time discretisations conserve energy, the resulting Picard iteration scheme does not. In the numerical tests below, we find that the number of Picard iterations required to achieve energy conservation up to machine precision is much higher than is usually considered in forecasting models. This suggests the use of simplifications to the fully discretised scheme, which lead to an additional energy error smaller than the error due to a small number of Picard iterations. Further, the temperature upwinded bracket presented in Definition 3 does not include upwinding in the velocity and density fields, leading to a non-satisfactory quality of the field development. In this section, we present a fully upwinded fully discretised formulation based on the bracket as described in Remark 1 and a small modification to the Poisson time discretisation.

In the fully upwinded bracket, we find that in the temperature advection equation the advecting and upwind velocities are given by $\mathbb{U}(\rho, \frac{\delta H}{\delta \mathbf{u}})$ and \mathbf{u} , respectively, which time-discretise within the Poisson integrator as $\overline{\frac{\delta H}{\delta \mathbf{u}}}$ (given by (3.1.4)) and $\bar{\mathbf{u}}$, respectively. The equations derived from the bracket can be simplified by ensuring that these two velocities are equal after time-discretisation, which can be achieved by time discretising the Hamiltonian variation in \mathbf{u} as

$$\frac{\delta H}{\delta \mathbf{u}} = P_{\mathbb{V}_u}(\rho \mathbf{u}) \quad \rightarrow \quad P_{\mathbb{V}_u}(\bar{\rho} \bar{\mathbf{u}}) =: \overline{\frac{\delta H}{\delta \mathbf{u}}} . \quad (3.2.1)$$

In this case, we find that the velocity recovery operator \mathbb{U} is evaluated as

$$\langle \bar{\rho} \mathbf{v}, \mathbb{U}(\bar{\rho}, \overline{\frac{\delta H}{\delta \mathbf{u}}}) \rangle = \langle \mathbf{v}, P_{\mathbb{V}_u}(\bar{\rho} \bar{\mathbf{u}}) \rangle = \langle \mathbf{v}, \bar{\rho} \bar{\mathbf{u}} \rangle \quad \forall \mathbf{v} \in \mathbb{V}_u, \quad (3.2.2)$$

so that

$$\mathbb{U}(\bar{\rho}, \overline{\frac{\delta H}{\delta \mathbf{u}}}) = \bar{\mathbf{u}}, \quad (3.2.3)$$

point-wise. With this in mind, we can replace the last terms in the thermal field part (2.4.35) - (2.4.36) of the fully upwinded bracket by

$$+ \langle \left(\widetilde{\frac{\delta H}{\delta \theta}} \right)_{\mathbf{u}}, \mathbb{S}_{\mathbf{u}}^{-1} \left(\theta^a \left(\mathbb{U} \left(\rho, \frac{\delta F}{\delta \mathbf{u}} \right) \right) \right) \rangle \quad \rightarrow \quad + \langle \left(\widetilde{\frac{\delta H}{\delta \theta}} \right)_{\mathbb{U}(\rho, \frac{\delta F}{\delta \mathbf{u}})}, \mathbb{S}_{\mathbf{u}}^{-1} (\theta^a(\mathbf{u})) \rangle \quad (3.2.4)$$

$$- \langle \left(\widetilde{\frac{\delta F}{\delta \theta}} \right)_{\mathbf{u}}, \mathbb{S}_{\mathbf{u}}^{-1} \left(\theta^a \left(\mathbb{U} \left(\rho, \frac{\delta H}{\delta \mathbf{u}} \right) \right) \right) \rangle \quad \rightarrow \quad - \langle \left(\widetilde{\frac{\delta F}{\delta \theta}} \right)_{\mathbb{U}(\rho, \frac{\delta H}{\delta \mathbf{u}})}, \mathbb{S}_{\mathbf{u}}^{-1} (\theta^a(\mathbf{u})) \rangle, \quad (3.2.5)$$

that is we swapped the advecting and upwind velocities. Note that this pair of terms is still bilinear and antisymmetric (given the upwind definition (2.3.10)). In the full Poisson integrator setup, we find that this modification of the bracket would lead to a thermal field equation whose modified test functions are upwinded inconsistently, in the sense that we would use $\bar{\mathbf{u}}$ for the test functions in the advection terms, but $\overline{\frac{\delta H}{\delta \mathbf{u}}}$ for the test function applied to the time derivative term. However, this is not the case for the simplified time-discretised form (3.2.1) of the Hamiltonian variation in \mathbf{u} , which is equal to $\bar{\mathbf{u}}$ point-wise. After swapping the velocities, we find that the double operator $\mathbb{S}_{\mathbf{u}}^{-1} \theta^a$ is not applied to a test function in the velocity equation anymore, so that the transpose formulation described in Proposition 2 is not needed anymore.

Proposition 3 *Consider the fully upwinded Poisson bracket as defined in remark 1, together with modification (3.2.4) - (3.2.5). Then applying the Poisson time discretisation (3.1.1) with modifica-*

tion (3.2.1) leads to a fully discretised set of equations of form

$$\langle \mathbf{w}, \mathbf{u}^{n+1} - \mathbf{u}^n \rangle - \Delta t \left(\langle \nabla^\perp (\bar{\rho} \mathbb{U}(\bar{\rho}, \mathbf{w}) \cdot \bar{\mathbf{u}}^\perp), \bar{\mathbf{u}} \rangle - \int_\Gamma \llbracket \bar{\rho} \mathbb{U}(\bar{\rho}, \mathbf{w}) \cdot \bar{\mathbf{u}}^\perp \rrbracket \mathbf{n}^\perp \cdot \tilde{\bar{\mathbf{u}}} dS \right) \quad (3.2.6)$$

$$+ \Delta t \left(\langle \bar{\rho} \mathbb{U}(\bar{\rho}, \mathbf{w}), f \bar{\mathbf{u}}^\perp \rangle + \langle \bar{\rho} \mathbb{U}(\bar{\rho}, \mathbf{w}), \nabla \frac{\bar{\delta H}}{\delta \rho} \rangle - \int_\Gamma \llbracket \frac{\bar{\delta H}}{\delta \rho} \mathbb{U}(\bar{\rho}, \mathbf{w}) \rrbracket \tilde{\bar{\rho}} dS \right) \quad (3.2.7)$$

$$- \Delta t L_{\mathbb{U}(\bar{\rho}, \mathbf{w})}^\theta \left(\bar{\theta}; \left(\frac{\bar{\delta H}}{\delta \theta} \right)_{\bar{\mathbf{u}}} \right) - \left\langle \left(\frac{\bar{\delta H}}{\delta \theta} \right)_{\mathbb{U}(\bar{\rho}, \mathbf{w})}, \theta^{n+1} - \theta^n \right\rangle = 0 \quad \forall \mathbf{w} \in \mathbb{V}_u, \quad (3.2.8)$$

$$\langle \phi, \rho^{n+1} - \rho^n \rangle - \langle \nabla \phi, \bar{\rho} \bar{\mathbf{u}} \rangle + \int_\Gamma \llbracket \phi \bar{\mathbf{u}} \rrbracket \tilde{\bar{\rho}} dS = 0 \quad \forall \phi \in \mathbb{V}_\rho, \quad (3.2.9)$$

$$\langle \gamma + \tilde{\gamma}_{\bar{\mathbf{u}}}, \theta^{n+1} - \theta^n \rangle + \Delta t L_{\bar{\mathbf{u}}}^\theta(\bar{\theta}; \gamma_{\bar{\mathbf{u}}}) = 0 \quad \forall \gamma \in \mathbb{V}_\theta. \quad (3.2.10)$$

Proof. All terms follow directly from the fully upwinded bracket together with the advecting velocity (3.2.3), except for the ones related to the modification (3.2.4) - (3.2.5). For the temperature SUPG related term (3.2.5), an argument identical to the one used in Proposition 1 can be used to arrive at the final form (3.2.10) of the thermal field equation. It remains to resolve the antisymmetric forcing term (3.2.4). Using the modified definition (2.4.37) of θ^a together with the definition (2.4.5) of \mathbb{S} , we can rewrite the thermal field equation (3.2.10) as a point-wise relation of form

$$\frac{\theta^{n+1} - \theta^n}{\Delta t} = \mathbb{S}_{\bar{\mathbf{u}}}^{-1}(\theta^a(\bar{\mathbf{u}})). \quad (3.2.11)$$

Replacing the corresponding term in (3.2.4), we arrive at the required form in (3.2.8). \square

Note that in this case, the density and thermal field equation correspond to their usual upwind form, together with a midpoint time discretisation rule. The antisymmetric structure now lies entirely in the velocity equation, with a forcing contribution of form (3.2.7) - (3.2.8) and a modified test function of form $\mathbb{U}(\bar{\rho}, \mathbf{w})$. Finally, as noted in remark 1, the above set of equations can be adjusted to three-dimensional scenarios by using velocity advection and Coriolis terms of form (2.4.39) - (2.4.40).

Remark 2 To solve for the velocity contribution (3.2.6) - (3.2.8) within the right-hand side \mathbf{R} of the Picard iteration scheme (3.1.9), we follow [26]. The treatment of the modified test functions $\mathbb{U}(\bar{\rho}, \mathbf{w})$ can be sketched as follows: writing the advection and forcing terms as $G(\mathbb{U}(\bar{\rho}, \mathbf{w}))$, we solve for $\mathbf{u}^* \in \mathbb{V}_u$ such that

$$\langle \bar{\rho} \mathbf{v}, \mathbf{u}^* \rangle = G(\mathbf{v}) \quad \forall \mathbf{v} \in \mathbb{V}_u. \quad (3.2.12)$$

Then in particular, given the definition of \mathbb{U} , we find that for any test function $\mathbf{w} \in \mathbb{V}_u$,

$$G(\mathbb{U}(\bar{\rho}, \mathbf{w})) = \langle \bar{\rho} \mathbb{U}(\bar{\rho}, \mathbf{w}), \mathbf{u}^* \rangle = \langle \mathbf{w}, \mathbf{u}^* \rangle, \quad (3.2.13)$$

and the velocity equation in the residual \mathbf{R} can be reformulated to

$$\mathbf{u}^{n+1,k} - \mathbf{u}^n + \mathbf{u}^*, \quad (3.2.14)$$

point-wise. In other words, considering (3.2.12) and the velocity equation (3.2.6) - (3.2.8), we find that this corresponds to solving for the velocity update using weighted test functions $\rho \mathbf{v}$.

Note that since the underlying bracket is still antisymmetric, the equation set formulated in Proposition 3 is energy conserving up to the time discretisation. The only difference to the fully energy

conserving Poisson integrator lies in the simplified variation of the Hamiltonian in \mathbf{u} , and comparing it to the non-simplified one, we find that

$$\frac{\overline{\delta H}}{\delta \mathbf{u}} - \frac{\overline{\delta H}'}{\delta \mathbf{u}} = \frac{1}{3} P_{\mathbb{V}_u} (\rho^n \mathbf{u}^n + \frac{1}{2} \rho^n \mathbf{u}^{n+1} + \frac{1}{2} \rho^{n+1} \mathbf{u}^n + \rho^{n+1} \mathbf{u}^{n+1}) - P_{\mathbb{V}_u} (\bar{\rho} \bar{\mathbf{u}}) \quad (3.2.15)$$

$$= \frac{1}{12} P_{\mathbb{V}_u} ((\rho^{n+1} - \rho^n)(\mathbf{u}^{n+1} - \mathbf{u}^n)) \quad (3.2.16)$$

$$= \frac{1}{12} P_{\mathbb{V}_u} ((\rho'^{n+1} - \rho'^n)(\mathbf{u}'^{n+1} - \mathbf{u}'^n)), \quad (3.2.17)$$

where $'$ denotes perturbation from the reference state. In particular, we therefore expect this modification to only have a small effect on the energy development, especially when only a small number of Picard iterations is used, so that the energy error is dictated by the error due to the linear solver.

Finally, compared to the equations derived from the bracket as presented in Definition 3, the equation set as given in Proposition 3 is fully upwinded and only requires additional projections for the Hamiltonian variations in ρ and θ . However, since these are projections into discontinuous and horizontally discontinuous spaces, the additional cost in evaluating the residual in each Picard iteration is small compared to similar discretisations derived in a non-Hamiltonian, non-energy conserving context.

3.3 Comparison to non-energy conserving space discretisations

For comparison purposes, we further describe two discretisations that are not energy conserving. The first is formulated such that the Poisson time integrator can be applied to it, allowing for a comparison that focuses on the exact energy conserving properties of the SUPG upwinded space discretisation. The second is formulated using a standard treatment of the Euler equations, and is used in comparison with the fully upwinded scheme as described in the previous section, with a smaller number of Picard iterations in the simulation runs.

For the first discretisation, we use a non-antisymmetric bracket of form

$$-\langle \frac{\delta F}{\delta \mathbf{u}}, \mathbf{q} \times \frac{\delta H}{\delta \mathbf{u}} \rangle + \langle \frac{\delta H}{\delta \rho}, \nabla \cdot \frac{\delta F}{\delta \mathbf{u}} \rangle - \langle \nabla \cdot \left(\frac{1}{\rho} \frac{\delta H}{\delta \theta} \frac{\delta F}{\delta \mathbf{u}} \right), \theta \rangle + \int_{\Gamma} \left[\frac{1}{\rho} \frac{\delta H}{\delta \theta} \frac{\delta F}{\delta \mathbf{u}} \right] \{\theta\} dS \quad (3.3.1)$$

$$- \langle \frac{\delta F}{\delta \rho}, \nabla \cdot \frac{\delta H}{\delta \mathbf{u}} \rangle - L_{\frac{\delta H}{\delta \mathbf{u}}/\rho}^{\theta} \left(\theta; \left(\frac{\delta F}{\delta \theta} \right)_{\mathbf{u}} \right) - \langle \left(\frac{\delta F}{\delta \theta} \right)_{\mathbf{u}}, \mathbb{S}_{\mathbf{u}}^{-1} \left(\theta^a \left(\frac{\delta H}{\delta \mathbf{u}} \right) \right) \rangle, \quad (3.3.2)$$

where $\{\cdot\}$ denotes the average across facets. Note that this bracket is antisymmetric with respect to the velocity and density advection terms, but not the thermal field advection term. The last two terms in (3.3.2) are set to arrive at the SUPG stabilised form (2.4.11) of the thermal field advection equation, while the last two terms of (3.3.1) correspond to a simple stabilisation of the non-upwinded thermal field bracket term:

$$\langle \frac{1}{\rho} \frac{\delta H}{\delta \theta} \nabla \theta, \frac{\delta F}{\delta \mathbf{u}} \rangle \rightarrow - \langle \nabla \cdot \left(\frac{1}{\rho} \frac{\delta H}{\delta \theta} \frac{\delta F}{\delta \mathbf{u}} \right), \theta \rangle + \int_{\Gamma} \left[\frac{1}{\rho} \frac{\delta H}{\delta \theta} \frac{\delta F}{\delta \mathbf{u}} \right] \{\theta\} dS, \quad (3.3.3)$$

which allows us to investigate the loss in energy due to a non-energy conserving implementation of the SUPG scheme.

The second discretisation is derived directly from the continuous Euler equations (2.1.22) - (2.1.24), disregarding the Hamiltonian framework. For this purpose, we use the same types of upwinding as

discussed in Section 2, i.e. standard DG upwinding for ρ , SUPG upwinding for θ , and upwinding for the rotational part of velocity advection. The resulting weak forms are then given by

$$\langle \mathbf{w}, \mathbf{u}_t \rangle - \langle \nabla^\perp (\mathbf{w} \cdot \mathbf{u}^\perp), \mathbf{u} \rangle + \int_\Gamma \llbracket \mathbf{w} \cdot \mathbf{u}^\perp \rrbracket \mathbf{n}^\perp \cdot \tilde{\mathbf{u}} \, dS - \langle \nabla \cdot \mathbf{w}, |\mathbf{u}|^2 \rangle - \langle \mathbf{w}, g\mathbf{k} \rangle \quad (3.3.4)$$

$$- c_p \langle \nabla \cdot (\theta \mathbf{w}), \pi \rangle + c_p \int_\Gamma \llbracket \theta \mathbf{w} \rrbracket \{\pi\} \, dS = 0 \quad \forall \mathbf{w} \in \mathbb{V}_u, \quad (3.3.5)$$

$$\langle \phi, \rho_t \rangle - \langle \nabla \phi, \rho \mathbf{u} \rangle + \int_\Gamma \llbracket \phi \mathbf{u} \rrbracket \tilde{\rho} \, dS = 0 \quad \forall \phi \in \mathbb{V}_\rho, \quad (3.3.6)$$

$$\langle \gamma + \tilde{\gamma}_\mathbf{u}, \theta_t \rangle + L_\mathbf{u}^\theta(\theta; \gamma_\mathbf{u}) = 0 \quad \forall \theta \in \mathbb{V}_\theta, \quad (3.3.7)$$

noting that for the Euler vertical slice test case considered below, the Coriolis parameter f is set zero. We use midpoint averages for the time discretisation, so that the resulting fully discretised density and thermal field equations are equal to the ones following from the approximately energy conserving discretisation (i.e. (3.2.9) and (3.2.10), respectively). On the other hand, we find that the velocity equation used here differs from the one given by (3.2.6) - (3.2.8) in that the forcing and advection terms have not been formulated with regards to antisymmetry and the variations of the Hamiltonian with respect to ρ and θ .

3.4 Test cases

Having formulated the Poisson bracket (Definition 3) and the Poisson integrator, as well as the simplified upwinded discretisation (Proposition 3) and two non-energy conserving schemes, we test for their energy-conserving properties and the qualitative field development. We first consider a thermal shallow water scenario and an Euler scenario, demonstrating energy conservation up to machine precision as well as an improved thermal field development when the SUPG scheme is applied. Given the shortcomings of the field development in the Euler scenario, we then move on to the fully upwinded setup, which we investigate using two Euler test cases.

3.4.1 Energy conservation and thermal field upwinding

The thermal shallow water test case considered here is based on the fifth test case in [25], corresponding to a spherical flow in geostrophic balance, perturbed by a mountain. Following [8], we set the buoyancy field accordingly to achieve a thermogeostrophic balance. The initial conditions are then given by

$$\mathbf{u} = u_0(-y, x, 0)/a, \quad (3.4.1)$$

$$\rho = h - (a\Omega u_0 + u_0^2/2) \frac{z^2}{ga^2} - b, \quad (3.4.2)$$

$$\theta = g \left(1 + \epsilon \left(\frac{\bar{\rho}}{\rho} \right)^2 \right), \quad (3.4.3)$$

where $b = b_0(1 - r/R)$ describes the mountain's surface, for $R = \pi/9$, mountain height $b_0 = 2000$ m and r such that $r = \min(R, \sqrt{(\lambda - \lambda_c)^2 + (\theta - \theta_c)^2})$. $\lambda \in [-\pi, \pi]$ and $\theta \in [-\pi/2, \pi/2]$ denote longitude and latitude respectively, and the mountain's centre is chosen as $\lambda_c = -\pi/2$ and $\theta_c = \pi/6$. The sphere's radius, its rotation rate, and the gravitational acceleration are given by $a = 6371220$ m, $\Omega = 7.292 \times 10^{-5} \text{ s}^{-1}$, and $g = 9.810616 \text{ ms}^{-2}$, respectively. Further, the mean height, the wind speed, and the buoyancy perturbation parameter are set to $\bar{\rho} = 5960$ m, $u_0 = 20$ m/s, and $\epsilon = 0.05$, respectively. Finally, for simplicity, we choose an SUPG parameter of form $\tau = \Delta t/2$; a further discussion on possible choices of τ can be found in [13].

The mesh is given by an icosahedral triangulation, where refinement level 0 corresponds to 20 triangles. For every higher level, each triangle is refined to 4 triangles (so that each increase corresponds to halving the cell side length Δx), and in this test case the refinement level was set to 4. The simulation is run for 50 days, with a time step of $\Delta t = 8$ minutes, and 8 Picard iterations for each time step.

The resulting buoyancy fields for the discretised equations corresponding to the non-upwinded bracket ((2.1.2) - (2.1.3)) and the buoyancy-upwinded bracket (Definition 3) are depicted in Figure 3. Further, the relative energy error (i.e. $(E_t - E_0)/E_0$) development for the aforementioned brackets as well as the non-energy conserving one ((3.3.1) - (3.3.2)) are depicted in Figure 4.

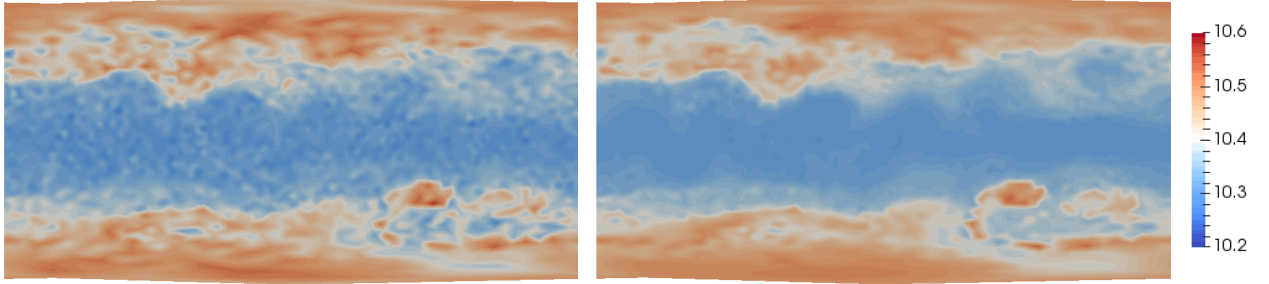


Figure 3: Buoyancy fields for thermal Williamson 5 test case after 50 days, for energy conserving discretisations. Left: no SUPG upwinding for buoyancy field; right: SUPG upwinding for buoyancy field. Mesh refinement level 4, $\Delta t = 8$ minutes, with 8 Picard iterations per time step.

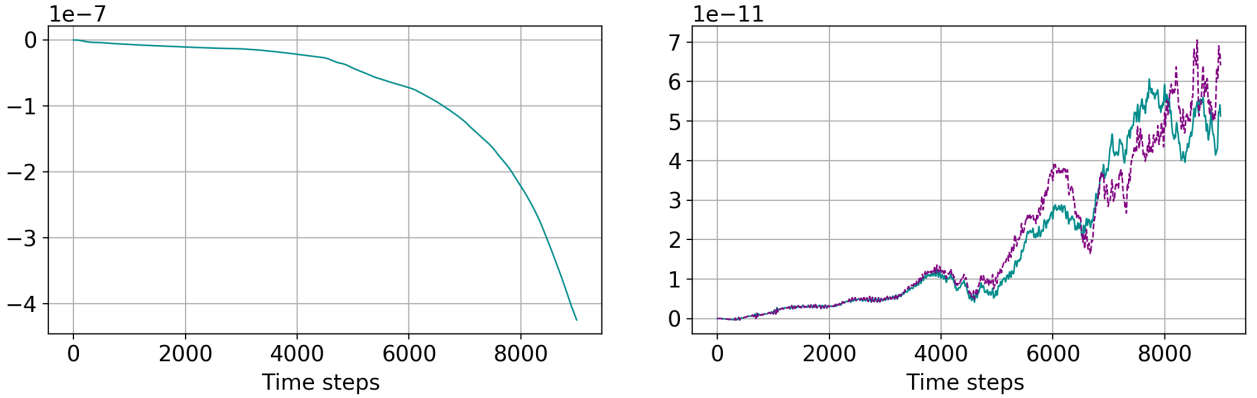


Figure 4: Relative energy error development for thermal Williamson 5 test case. Left: non-energy conserving bracket. Right: energy conserving bracket with SUPG for buoyancy (cyan) and energy conserving bracket without SUPG for buoyancy (dashed purple).

As expected, we find that the incorporation of the SUPG scheme markedly reduces the occurrence of spurious oscillations in the buoyancy field development. Further, both energy conserving brackets lead to energy convergence up to solver tolerance, with an improvement by 4 orders of magnitude when compared to the non-antisymmetric bracket.

Next, we consider the brackets in an Euler equations scenario. For this purpose, we use the next

to lowest order density finite element space ($r=1$) and the corresponding spaces for the other fields as described in Section 2.2.1. To ensure a stable field development, the non-upwinded bracket is replaced by one that includes DG-upwinding for potential temperature in the horizontal (but no SUPG scheme for the vertical). The test case is given by a falling bubble in a vertical slice of the atmosphere, based on one as described in [24]. For this purpose, we consider a horizontally periodic rectangular domain Ω of 32 km length and 6.4 km height, with a constant potential temperature background field $\bar{\theta} = 300$ K and corresponding pressure and density fields in hydrostatic balance. A temperature perturbation of form

$$\Delta T = \begin{cases} -\frac{15}{2}(1 + \cos(r\pi)) & \text{if } r < 1, \\ 0 & \text{otherwise,} \end{cases} \quad r = \sqrt{\frac{(x - x_c)^2}{x_r^2} + \frac{(z - z_c)^2}{z_r^2}}, \quad (3.4.4)$$

is added to the background potential temperature, while the density field is left unperturbed. The perturbation's horizontal and vertical centre and radius are given by $(x_c, x_r) = (16, 4)$ and $(z_c, z_r) = (3, 2)$ kilometres, respectively. The gravitational acceleration is defined as in the thermal shallow water test case, and the remaining physical parameters are given by $c_v = 716.5 \text{ m}^2\text{s}^{-2}\text{K}^{-1}$, $R = 287 \text{ m}^2\text{s}^{-2}\text{K}^{-1}$, and $p_0 = 100 \text{ kPa}$. Finally, we note that a constant viscosity term is commonly added to the continuous equations in this test case to obtain a solution that converges as the resolution is refined [17]. In our case, we do not include this term due to our focus on energy conservation.

The mesh is given by a vertically extruded interval mesh, with horizontal and vertical resolutions equal to $\Delta x = \Delta z = 100 \text{ m}$. The simulation is run for 900 seconds, with a time step of $\Delta t = 0.5 \text{ s}$, and 32 Picard iterations for each time step.

To focus on the effects of upwinding, we consider the field development after 400 and 800 seconds. The resulting images and relative energy error developments are depicted in Figures 5 and 6, in an arrangement equal to the one for the thermal shallow water equations above.

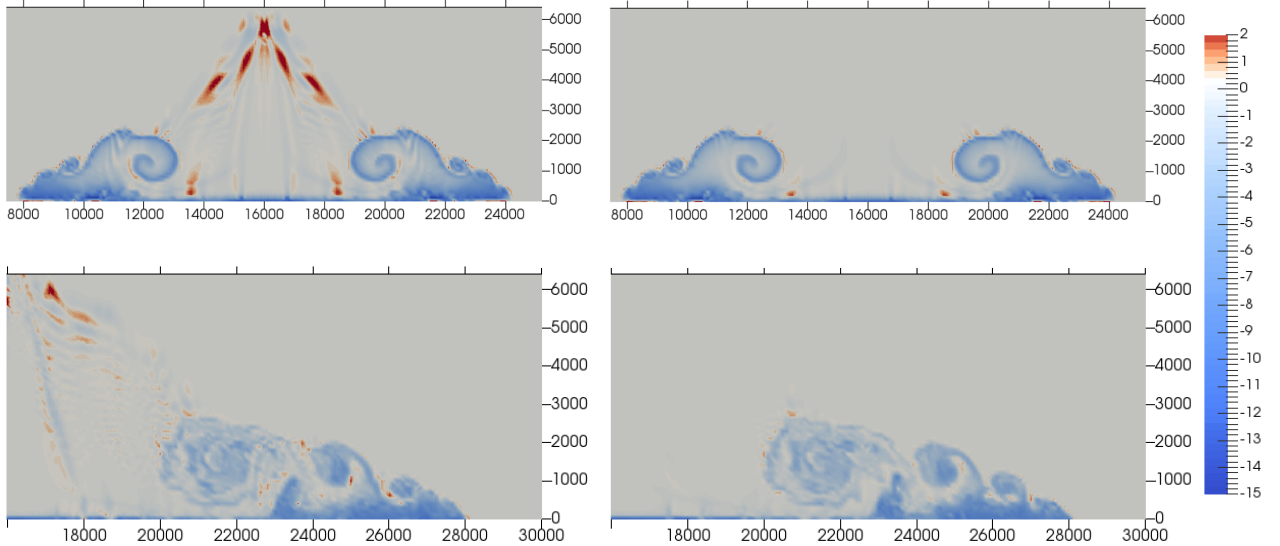


Figure 5: Potential temperature fields for falling bubble test case after 400 s (top row) and 800 s (bottom row), for energy conserving discretisations. Left column: no SUPG upwinding for potential temperature field; right column: SUPG upwinding for potential temperature field. $\Delta x = \Delta z = 100 \text{ m}$, $\Delta t = 0.5 \text{ s}$, with 32 Picard iterations per time step.

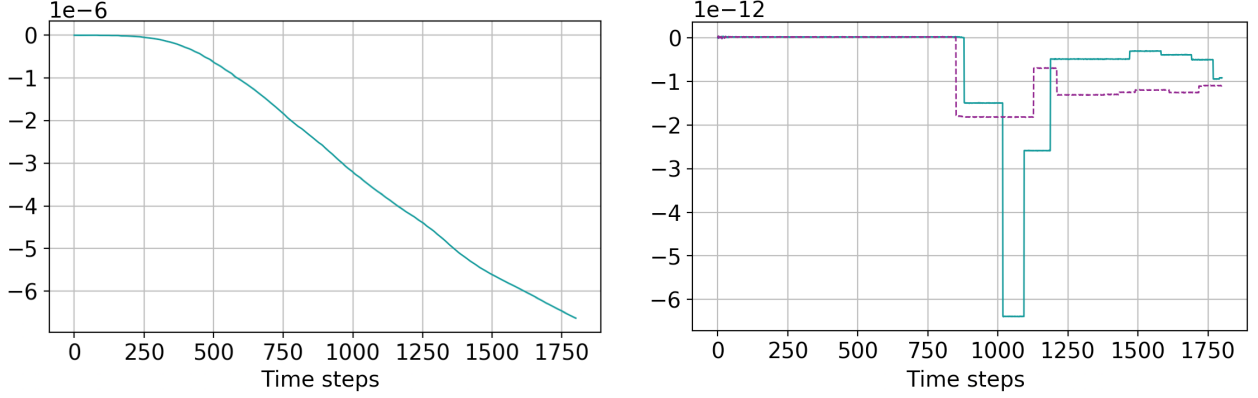


Figure 6: Relative energy error development for falling bubble test case. Left: non-energy conserving bracket. Right: energy conserving bracket with SUPG for buoyancy (cyan) and energy conserving bracket without SUPG for buoyancy (dashed purple).

We find that if no SUPG scheme is applied in the vertical direction of potential temperature transport, spurious upward moving features occur in the potential temperature field development near the centre of the domain, where the bubble falls towards the bottom boundary. In the presence of an SUPG scheme these features are removed, again indicating a qualitatively favourable field development if such a scheme is included. Further, as expected, energy is conserved up to solver tolerance for the two energy conserving brackets, with occasional jumps likely due to an insufficient number of Picard iterations. In contrast, the non-energy conserving bracket leads to a loss of energy of the order of 10^{-6} , 6 orders of magnitude larger than the energy conserving ones.

3.4.2 Fully upwinded, approximately energy conserving scheme

While including an SUPG scheme for the potential temperature advection leads to an improvement of the field development, the latter still suffers from an absence of upwinding in the other fields, leading to an insufficient resolution of the density current flowing along the bottom boundary. Further, 32 Picard iterations were required to achieve energy conservation of the order of 10^{-12} . We therefore next consider the field and energy error developments for the simplified fully upwinded scheme as presented in Proposition 3, which is energy conserving in space and energy conserving in time up to the difference given by (3.2.17). The test cases considered here are given by the falling bubble one as described above, as well as a rising bubble test case based on [5]. The latter is prone to secondary plumes (see e.g. [2]), and to avoid these in our discussion here, we consider the next higher order set of finite element spaces ($r=2$) for this test case. The domain Ω is given by a horizontally periodic square of 10 km side length. The background fields are given as in the falling bubble case, and the initial temperature perturbation is given by

$$\Delta\theta = \begin{cases} 2 \cos^2(\frac{r\pi}{2}) & \text{if } r < 1, \\ 0 & \text{otherwise,} \end{cases} \quad (3.4.5)$$

for r as in (3.4.4) above, with $(x_c, x_r) = (5, 2)$ and $(z_c, z_r) = (2, 2)$ kilometres, respectively. As before, the density field is left unperturbed. The mesh is as for the falling bubble test case with $\Delta x = \Delta z = 100$ m for the relative energy error study below, and a higher resolution of $\Delta x = \Delta z = 50$ m for the field development figures below. The simulations are run for 1000 seconds, with a time step of $\Delta t = 1$ s for the 100 m mesh and $\Delta t = 0.5$ s for the 50 m mesh.

First, we compare the impact of both the reduced number of Picard iterations and the approximated Poisson integrator (i.e. (3.2.1)) on the relative energy error development. For this purpose, we run the falling and rising bubble test cases for $k \in \{4, 5, 6, 8\}$ Picard iterations, each time for both the fully energy conserving Poisson integrator and the approximated version as given in Proposition 3. The resulting energy developments are depicted in Figure 7.

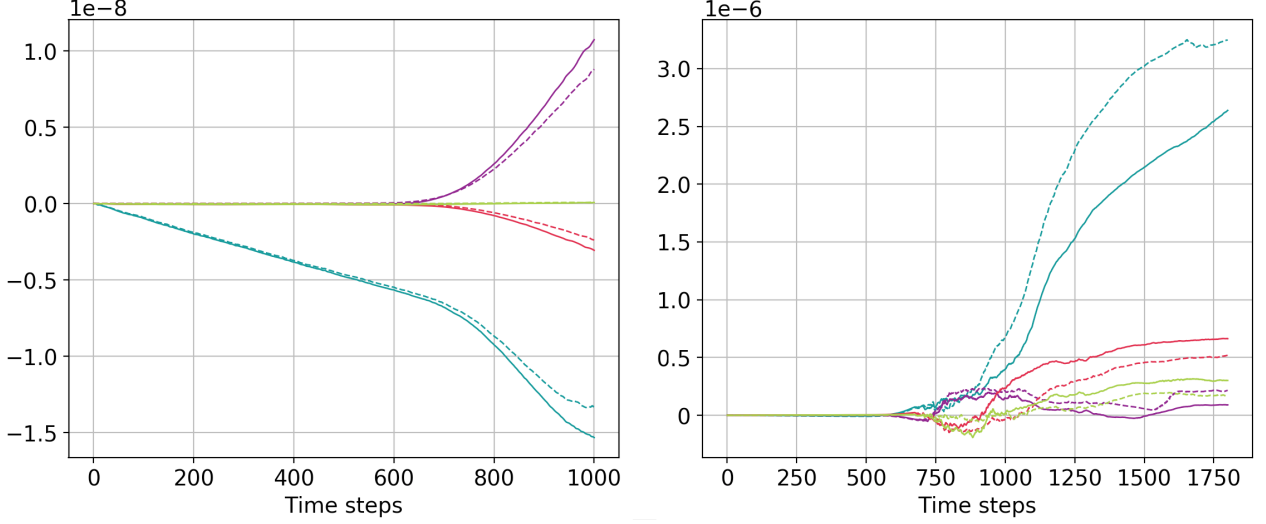


Figure 7: Relative energy error development for rising (left) and falling (right) bubble test cases. Solid lines indicate midpoint approximation, dashed ones the full Poisson integrator. Colours correspond to cyan for 4 Picard iterations, purple for 5, red for 6, and light green for 8.

While more evident for the less turbulent rising bubble test case, we find that in both cases the choice of number of Picard iterations dominates the relative energy error development when compared to whether or not the Poisson integrator has been approximated. In particular, this indicates that the approximated scheme as given in Proposition 3 does not lead to a substantial increase in energy error when a small number of Picard iterations is used, suggesting that the approximation (and therefore the removal of the additional calculations for \mathbb{U} , $(\mathbb{S}_{\mathbf{u}}^{-1})^*$, and $(\theta^a)^*$ appearing in the fully upwinded, fully energy conserving discretisation) is justified.

To test the improvement of the qualitative field development when a fully upwinded bracket is used, we compare the scheme as given in Proposition 3 with a fully upwinded reference scheme not derived in a Hamiltonian setup, as defined in (3.3.5) - (3.3.7). Further, we also consider the energy development for this setup, using 4 Picard iterations in each time step. Note that considering the two discretisations, we find that the only additional computational cost of the approximately energy conserving scheme lies in computing $\frac{\delta H}{\delta \rho}$ and $\frac{\delta H}{\delta \theta}$ for each Picard iteration, i.e. a DG space and a horizontally DG space projection. The resulting falling and rising bubble potential temperature fields are depicted in Figure 8, and the corresponding energy plots can be found in Figure 9.

For the rising bubble test case, we find a virtually identical field development. In terms of the relative energy error, we can divide the bubble's evolution into an initial phase, where the bubble starts rising, and a later phase, in which two vortices are formed at the bubble's lower ends. For the former phase, the approximately energy conserving setup suffers from a small, constant decrease in

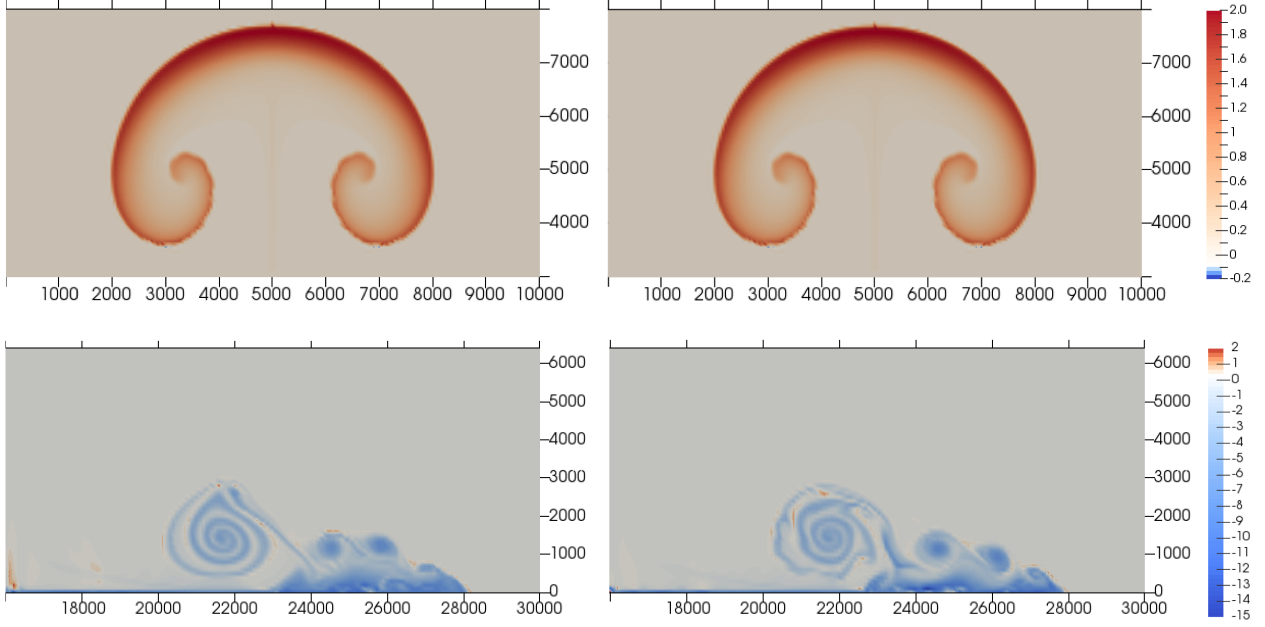


Figure 8: Potential temperature fields for energy conserving scheme with midpoint approximation (left column) and non-energy conserving scheme (right column). Top: rising bubble test case at 1000 s. Bottom: falling bubble test case at 800 s.

energy, probably related to the initial adjustment of the unperturbed density field to a perturbed state (in the sense that if a corresponding perturbation to the density field is added to the initial conditions, this decrease disappears). Once the vortices start to form, however, the non-energy conserving setup suffers from a much larger increase in relative energy error than the approximately energy conserving one does, leading to a final energy error larger by almost an order of magnitude.

Similarly, we find an improved energy conservation by nearly an order of magnitude for the falling bubble test case. Additionally, we observe a qualitatively different field development, where the higher degree of energy conservation leads to the formation of additional smaller vortices in the main vortex. This demonstrates that even in simulations with a comparable computational effort, the approximately energy conserving discretisation still leads to a significant reduction in the relative energy error in comparison to a corresponding non-Hamiltonian discretisation, which in turn may influence the field development. Further, should a higher degree of energy conservation be required (albeit at a higher computational cost), this can readily be achieved in the approximately energy conserving setup by using a moderately higher number of Picard iterations (with another order of magnitude gained for 6 iterations, as indicated in Figure 7).

4 Conclusion

In this paper, we presented an almost Poisson bracket discretisation using the compatible finite element method, which includes an SUPG scheme for the thermal field advection. The SUPG formulation relies on moving the upwinded part of the test function corresponding to the temperature time derivative into the Poisson bracket. In view of the Poisson time integration scheme, a temperature advection and an SUPG upwinding related operator were introduced in order to reformulate the thermal field time derivative term occurring in the bracket. We demonstrated how to recover the thermal and velocity field evolution equations given the SUPG-modified bracket, showing that the

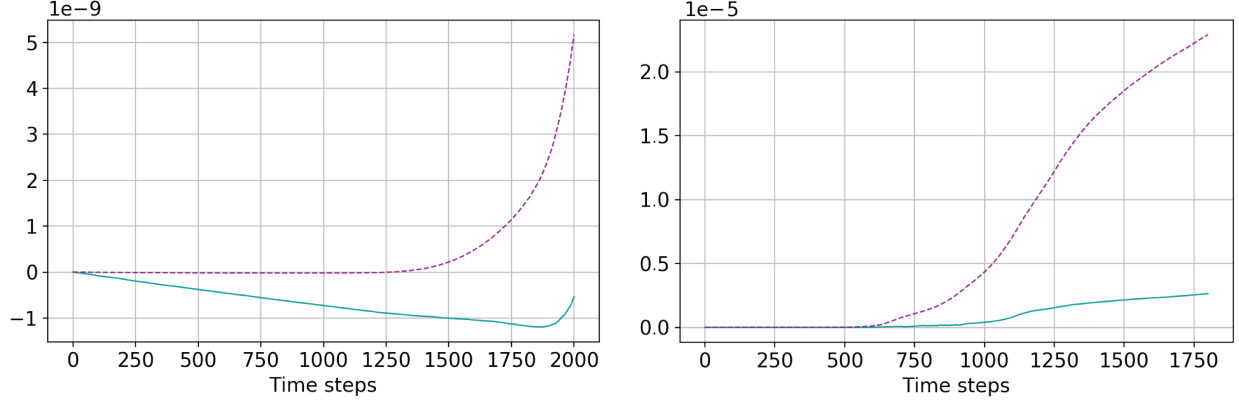


Figure 9: Relative energy error development for energy conserving scheme with midpoint approximation (cyan) and non-energy conserving scheme (dashed purple), for 4 Picard iterations per time step. Left: rising bubble test case. Right: falling bubble test case.

former corresponds to the usual SUPG formulation of a transport equation with the given underlying finite element spaces. Further, for the interest of a fully upwinded, computationally less costly discretisation, we introduced an approximately energy conserving version including upwinding in the density and velocity fields.

In numerical tests, we demonstrated energy conservation up to solver tolerance for the SUPG-modified bracket for an Euler and a thermal rotating shallow water scenario. Further, the incorporation of the SUPG scheme was shown to lead to a significant improvement of the qualitative thermal field development in both cases. Finally, we considered the approximately energy conserving discretisation in a simulation with a small number of Picard iterations, showing that we still gain a reduced energy error when compared to a reference discretisation derived in a non-Hamiltonian setup, leading to a qualitatively different field development for one of the two considered Euler test cases.

In future work, we aim to compare different upwind schemes within the Hamiltonian framework. In particular, this includes the choice of velocity advection scheme, which can either be formulated using upwinding for velocity, or an upwinded formulation for vorticity as presented for the shallow water equations in [1]. While the numerical tests for the SUPG scheme considered here were restricted to two dimensions, this comparison would ideally be done in a fully three-dimensional setting.

References

- [1] W. Bauer and C. J. Cotter. Energy–enstrophy conserving compatible finite element schemes for the rotating shallow water equations with slip boundary conditions. *Journal of Computational Physics*, 373:171 – 187, 2018.
- [2] T. M. Bendall, T. H. Gibson, J. Shipton, C. J. Cotter, and B. Shipway. A Compatible Finite Element discretisation for the moist compressible Euler equations. *arXiv preprint arXiv:1910.01857*, 2019.
- [3] G.-T. Bercea, A. T. T. McRae, D. A. Ham, L. Mitchell, F. Rathgeber, L. Nardi, F. Luporini, and P. H. J. Kelly. A structure-exploiting numbering algorithm for finite elements on extruded meshes, and its performance evaluation in Firedrake. *arXiv preprint arXiv:1604.05937*, 2016.
- [4] A. N. Brooks and T. J. R. Hughes. Streamline upwind/Petrov-Galerkin formulations for convection dominated flows with particular emphasis on the incompressible Navier-Stokes equations. *Computer methods in applied mechanics and engineering*, 32(1-3):199–259, 1982.
- [5] R. L. Carpenter Jr, K. K. Droegemeier, P. R. Woodward, and C. E. Hane. Application of the piecewise parabolic method (PPM) to meteorological modeling. *Monthly Weather Review*, 118(3):586–612, 1990.
- [6] D. Cohen and E. Hairer. Linear energy-preserving integrators for Poisson systems. *BIT Numerical Mathematics*, 51(1):91–101, 2011.
- [7] C. J. Cotter and J. Shipton. Mixed finite elements for numerical weather prediction. *Journal of Computational Physics*, 231(21):7076 – 7091, 2012.
- [8] C. Eldred, T. Dubos, and E. Kritsikis. A quasi-Hamiltonian discretization of the thermal shallow water equations. *Journal of Computational Physics*, 379:1 – 31, 2019.
- [9] R. Ford, M. J. Glover, D. A. Ham, C. M. Maynard, S. M. Pickles, G. Riley, and N. Wood. Gung Ho: A code design for weather and climate prediction on exascale machines. In *Proceedings of the Exascale Applications and Software Conference*, 2013.
- [10] A. Gassmann. A global hexagonal C-grid non-hydrostatic dynamical core (ICON-IAP) designed for energetic consistency. *Quarterly Journal of the Royal Meteorological Society*, 139(670):152–175, 2013.
- [11] T. H. Gibson, L. Mitchell, D. A. Ham, and C. J. Cotter. Slate: extending Firedrake’s domain-specific abstraction to hybridized solvers for geoscience and beyond. *arXiv preprint:1802.00303*, 2018.
- [12] M. Homolya, L. Mitchell, F. Luporini, and D. A. Ham. TSFC: a structure-preserving form compiler. *SIAM Journal on Scientific Computing*, 40(3):C401–C428, 2018.
- [13] D. Kuzmin. A guide to numerical methods for transport equations. *University Erlangen-Nuremberg*, 2010.
- [14] D. Lee and A. Palha. A mixed mimetic spectral element model of the 3D compressible Euler equations on the cubed sphere. *Journal of Computational Physics*, 401:108993, 2020.
- [15] F. Luporini, D. A. Ham, and P. H. J. Kelly. An algorithm for the optimization of finite element integration loops. *ACM Trans. Math. Softw.*, 44(1):3:1–3:26, March 2017.

- [16] T. Melvin, T. Benacchio, J. Thuburn, and C. J. Cotter. Choice of function spaces for thermodynamic variables in mixed finite-element methods. *Quarterly Journal of the Royal Meteorological Society*, 144(712):900–916, 2018.
- [17] Thomas Melvin, Mark Dubal, Nigel Wood, Andrew Staniforth, and Mohamed Zerroukat. An inherently mass-conserving iterative semi-implicit semi-Lagrangian discretization of the non-hydrostatic vertical-slice equations. *Quarterly Journal of the Royal Meteorological Society*, 136(648):799–814, 2010.
- [18] P. J. Morrison. Hamiltonian description of the ideal fluid. *Reviews of modern physics*, 70(2):467, 1998.
- [19] A. Natale and C. J. Cotter. A variational H(div) finite element discretisation for perfect incompressible fluids. *IMA Journal of Numerical Analysis*, 38(3):1388–1419, 2017.
- [20] A. Natale, J. Shipton, and C. J. Cotter. Compatible finite element spaces for geophysical fluid dynamics. *Dynamics and Statistics of the Climate System*, 1(1), 2016.
- [21] F. Rathgeber, D. A. Ham, L. Mitchell, M. Lange, F. Luporini, A. T. T. McRae, G. T. Bercea, G. R. Markall, and P. H. J. Kelly. Firedrake: automating the finite element method by composing abstractions. *ACM Transactions on Mathematical Software (TOMS)*, 43(3):24, 2016.
- [22] T. G. Shepherd. Symmetries, conservation laws, and Hamiltonian structure in geophysical fluid dynamics. *Adv. Geophys*, 32(287-338):2, 1990.
- [23] J. Shipton, T. H. Gibson, and C. J. Cotter. Higher-order compatible finite element schemes for the nonlinear rotating shallow water equations on the sphere. *Journal of Computational Physics*, 375:1121–1137, 2018.
- [24] J. M. Straka, R. B. Wilhelmson, L. J. Wicker, J. R. Anderson, and K. K. Droegemeier. Numerical solutions of a non-linear density current: A benchmark solution and comparisons. *International Journal for Numerical Methods in Fluids*, 17(1):1–22, 1993.
- [25] D. L. Williamson, J. B. Drake, J. J. Hack, R. Jakob, and P. N. Swarztrauber. A standard test set for numerical approximations to the shallow water equations in spherical geometry. *Journal of Computational Physics*, 102(1):211–224, 1992.
- [26] G. A. Wimmer, C. J. Cotter, and W. Bauer. Energy conserving upwinded compatible finite element schemes for the rotating shallow water equations. *Journal of Computational Physics*, page 109016, 2019.